Low Noise Research Fan Stage Design

David E. Hobbs, Robert J. Neubert, Eric W. Malmborg, Daniel H. Philbrick, and David A. Spear
United Technologies Corporation, Pratt & Whitney, East Hartford, Connecticut

The NASA STI Program Office ... in Profile

Since its founding, NASA has been dedicated to the advancement of aeronautics and space science. The NASA Scientific and Technical Information (STI) Program Office plays a key part in helping NASA maintain this important role.

The NASA STI Program Office is operated by Langley Research Center, the lead center for NASA's scientific and technical information. The NASA STI Program Office provides access to the NASA STI Database, the largest collection of aeronautical and space science STI in the world. The Program Office is also NASA's institutional mechanism for disseminating the results of its research and development activities. These results are published by NASA in the NASA STI Report Series, which includes the following report types:

- TECHNICAL PUBLICATION. Reports of completed research or a major significant phase of research that present the results of NASA programs and include extensive data or theoretical analysis. Includes compilations of significant scientific and technical data and information deemed to be of continuing reference value. NASA counter-part of peer reviewed formal professional papers, but having less stringent limitations on manuscript length and extent of graphic presentations.

- TECHNICAL MEMORANDUM. Scientific and technical findings that are preliminary or of specialized interest, e.g., quick release reports, working papers, and bibliographies that contain minimal annotation. Does not contain extensive analysis.

- CONTRACTOR REPORT. Scientific and technical findings by NASA-sponsored contractors and grantees.

- CONFERENCE PUBLICATION. Collected papers from scientific and technical conferences, symposia, seminars, or other meetings sponsored or co-sponsored by NASA.

- SPECIAL PUBLICATION. Scientific, technical, or historical information from NASA programs, projects, and missions, often concerned with subjects having substantial public interest.

- TECHNICAL TRANSLATION. English-language translations of foreign scientific and technical material pertinent to NASA's mission.

Specialized services that help round out the STI Program Office's diverse offerings include creating custom thesauri, building customized databases, organizing and publishing research results ... even providing videos.

For more information about the NASA STI Program Office, you can:

- Access the NASA STI Program Home Page at http://www.sti.nasa.gov STI-homepage.html

- E-mail your question via the Internet to help@sti.nasa.gov

- Fax your question to the NASA Access Help Desk at (301) 621-0134

- Phone the NASA Access Help Desk at (301) 621-0390

- Write to:
  NASA Access Help Desk
  NASA Center for AeroSpace Information
  7121 Standard Drive
  Hanover, MD 21076

NASA Contractor Report 195382

Low Noise Research Fan Stage Design

David E. Hobbs, Robert J. Neubert, Eric W. Malmborg, Daniel H. Philbrick, and David A. Spear
United Technologies Corporation, Pratt & Whitney, East Hartford, Connecticut

National Aeronautics and
Space Administration

Lewis Research Center

March 1995

Available from

TABLE OF CONTENTS

LIST OF ILLUSTRATIONS

Page

LIST OF TABLES

Page

SUMMARY

This report describes the design of the Low Noise Research Fan stage. The fan is a variable pitch design which is designed at the cruise pitch condition. Relative to the cruise setting, the blade is closed at takeoff and opened for reverse thrust operation. The fan stage is a split flow design with fan exit guide vanes (FEGVs) and core stators.

The fan stage design was combined with a nacelle and engine core duct to form a powered fan/nacelle subscale model. This model is intended for use in aerodynamic performance, acoustic and structural testing in a wind tunnel. The model has a 22-in. outer fan diameter and a hub-to-tip ratio of 0.426, which permits the use of existing NASA fan and cowl force balance designs and rig drive systems. The design parameters were selected to permit valid acoustic and aerodynamic comparisons with the Pratt & Whitney 17-in. rig previously tested under NASA contract.

The fan stage design is described in detail. The results of the design axisymmetric analysis at aerodynamic design condition are included. The structural analysis of the fan rotor and attachment is described including the material selections and stress analysis. The blade and attachment are predicted to have adequate low cycle fatigue life and an acceptable operating range without resonant stress or flutter.

The stage was acoustically designed with airfoil counts in the FEGV and core stator to minimize noise. A fan/FEGV tone analysis developed separately under NASA contract was used to determine these airfoil counts.

The fan stage design was matched to a nacelle design to form a fan/nacelle model for wind tunnel testing. The nacelle design was developed under a separate NASA contract. The nacelle was designed with an axisymmetric inlet, cowl, and nozzle for convenience in testing and fabrication. Aerodynamic analysis of the nacelle confirmed the required performance at various aircraft operating conditions.

1. INTRODUCTION

Major airports in the nation's air transportation system face a serious problem in providing greater capacity to meet the ever increasing demands of air travel. This problem could be relieved if airports are allowed to increase their operating time, now restricted by curfews and by relaxing present limits on takeoff and landings. The key operational issue in extending the present curfews is noise.

A recent study of this problem, conducted under NASA contract NAS3-25952 (Aero Propulsion Technology) Task V, focused on new engine ultra high bypass propulsor technologies, which would significantly reduce noise. This study also investigated the aero/acoustic/structural advancements in fan and nacelle technologies required to reduce noise 5 to 10 EPNDB relative to FAR 36 Stage 3 at each of the three measurement stations: takeoff (cutback), approach, and sideline. Major emphasis focused on fan blade aero/acoustic and structural technology evaluations that led to the definition of specific technology verification plans to demonstrate this technology.

As planned, many of these selected technologies have been incorporated in a subscale fan/nacelle model, which will be used in testing to confirm the value of these concepts. This report describes the aerodynamic, acoustic, and structural design of this model.

2. FAN STAGE AERODYNAMIC DESIGN

2.1 Objective

This fan was designed to model a low noise research fan stage for use in combined acoustic, aerodynamic, and nacelle testing. The low noise fan stage was designed to reduce noise approximately 11 dB cumulative, relative to current technology fans at the same takeoff pressure ratio. This was achieved by lowering tip speed at takeoff. Operability was maintained by making use of casing treatment and variable pitch. The fan design parameters were selected to make it representative of current fans. The main design constraint was hub-to-tip radius ratio which was limited to 0.426 by the nacelle rig, drive model force balance system, and space for an adjustable pitch disk.

2.2 Fan Stage Design Parameter Selection

The fan stage design parameter selection was based on fulfilling the following requirements:

- Application of the advanced technology concepts developed in the previous design study under Aero Propulsion Technology Contract, Task V[1]

- Application of the advanced technology concepts to lower noise

- Geometric compatibility with the new NASA Lewis Research Center (LeRC) 22-in. air drive turbine rig cowl and fan force balance diameters.

The primary technology used was lower rotor speed relative to the current fan design practice, Figure 2-1. This reduction of speed was made possible by the application of casing treatment and variable pitch. The hub-to-tip radius ratio was set at 0.426, permitting the use of the NASA LeRC 22-in. rig cowl and fan balance designs. Airfoil counts were chosen to minimize noise, based on an acoustic analysis.

The major innovation in this design is the reduction of rotor speed at takeoff. This leads to an expected noise reduction of 11dB cumulative, and the opportunity to significantly reduce the weight of the rotating system and containment case.

The considerations above have led to the final design parameter selection for the low noise fan. These design parameters are shown in Table 2-1 compared to the 17-in. fan/nacelle model.

---

[1] Holcombe, Vincent, *Low Noise Engine Definition Study*, Aero-Propulsion Technology (APT) Task V, NAS3 25952 Contract with United Technologies Corp., March, 1991.

2.3 Fan Blade Design at Cruise

Table 2-1 compares the low noise fan design parameters to the 17-in. fan model.

Table 2-1. Fan Design Parameters

Fan Parameters	Fan/Nacelle 17 in. Rig	P&W-NASA Low Noise
Pr (Duct, Stage)		
• SLTO	1.20	1.284
• Cruise	1.21	1.294
• Approach	-	1.077
• Cutback	-	1.209
RPM (ft/sec)		
• SLTO	11,675	8750
• Cruise	11,200	8400
• Approach	-	5000
• Cutback	-	7740
U_{tip} Corr (ft/sec)		
• SLTO	836	840
• Cruise	802	806
• Approach	-	480
• Cutback	-	743
W/A Corr (lbm/sec ft^2)		
• SLTO	32.6	36.9
• Cruise	40.8	42.5
• Approach	-	22.7
• Cutback	-	33.3
Bypass Ratio - Cruise	20.4	13.3
Blade Number	16	18
Vane Number	22/40	45
Hub/Tip	0.443	0.426
Diameter - LE	17.0	22.0

See Appendix A for design velocity vectors and Appendix B for flow path coordinates.

2.4 Fan Blade Airfoil Sections

Controlled diffusion airfoil[2] sections were used for the fan rotor. Airfoil section parameters were optimized for good performance as shown in Figure 2-2.

At cruise and takeoff operating line conditions, all airfoil sections were predicted to be free of boundary layer separation at all spans. In addition, all sections were predicted to be separation free at the takeoff stall line and maximum flow condition, verifying they could meet incidence and loading requirements (see Figure 2-3).

---

[2] Hobbs, D.E. and H.D. Weingold, *Development of Controlled Diffusion Airfoils for Multistage Compressor Applications*, ASME Journal of Engineering for Gas Turbines and Power, Vol. 106, 1984, pp. 271-278.

A Navier-Stokes analysis of the fan rotor confirmed it to be separation free full span, Figure 2-4 and Figure 2-5. The Navier-Stokes analysis is described in more detail in Section 5 of this report.

2.5 Casing Treatment Design

Previous Pratt & Whitney fan testing has verified that casing treatment can improve fan operability. The low noise configuration is based on these previous designs scaled to the low noise fan tip speed and pressure ratio. The objective was to obtain the same operability as current fans.

2.6 Model Flowpath

The internal model fan duct flowpath is shown in Figure 2-6. The inner wall was constrained by the rig drive and force balance system. The bypass-core flow splitter radial location was determined by fan bypass ratio and axial location by core dirt ingestion and acoustic spacing criteria.

2.7 FEGV Design

The nominal FEGV spacing is 1.8 times the fan axial mid span chord (bx). The acoustic test program for this model includes testing with the FEGV moved forward to 1.16 times fan bx and rearward to 2.6 times fan bx.

The number of FEGVs and axial locations was determined from acoustic considerations. Aspect ratio and thickness-to-chord ratio (t/b) were taken from structural studies. The number of FEGVs was determined with the acoustic analysis in Section 4 of this report. The FEGV section design was optimized for minimum loss and stall incidence requirements, Figure 2-7.

An FEGV design was also made for a flowpath which does not have core flow capability. A different FEGV design was required because the inlet gas angle was significantly different than for the core flow nacelle model FEGV, Figure 2-8. Figure 2-9 shows the section Mach contours at design point and at stall incidence. The no core flow fan duct flowpath is shown in Figure 2-10. The outer wall was selected to be consistent with the nacelle model, except for moving the stator further aft, to allow for laser doppler velocimetry wake measurements, three axial fan mid span chords downstream.

2.8 Core Stator Design

The core stator design is unique to this model since there is no downstream low pressure compressor and the flowpath was constrained by the rig drive system. Therefore, it was designed conservatively to ensure that it does not restrict rig testing

2.9 Core Duct Flow

This fan stage design properly models the engine core inlet. This core inlet is important because, without the removal of the core flow, the FEGV cannot be designed with airfoil sections representative of engine applications. In addition, wakes of the fan hub airfoil sections, which normally pass into the core, impinge on the FEGVs creating an additional noise source not found in engine applications.

Two core flow capabilities were designed for this model. The first design is a passive through-flow configuration which used the fan hub pressure ratio to pump the flow through the core ducting, a diffuser and back out into the wind tunnel. In the second design, the flow is pulled through the core inlet by a tunnel vacuum system. In this case, the same core duct is attached to an annular collecting plenum which is connected to the tunnel vacuum piping. The passive system will be used in all the forward thrust testing if flows are high enough; the vacuum system will be used in the reverse thrust testing, since, in this configuration, the fan is not pumping flow into the core. The vacuum system could also be used in the forward thrust testing to achieve the desired core flows.

2.10 Unsteady Aerodynamic Analysis Airfoil Counts

In this current fan stage and casing treatment design, a conscious effort was made to select the number of airfoils to permit efficient future unsteady analysis. Since the number of fan blades had been selected as eighteen, for structural reasons, the numbers of the stationary airfoils were selected as multiples of nine to reduce the number of airfoils interacting in periodic groups to a minimum. Thus, the unsteady flow problem can be reduced exactly to a computational model of two blades, forming one passage, interacting with five FEGVs, and seven core stators. This Low noise fan/nacelle model will offer a unique opportunity to compare unsteady pressure and temperature measurements to analysis results.
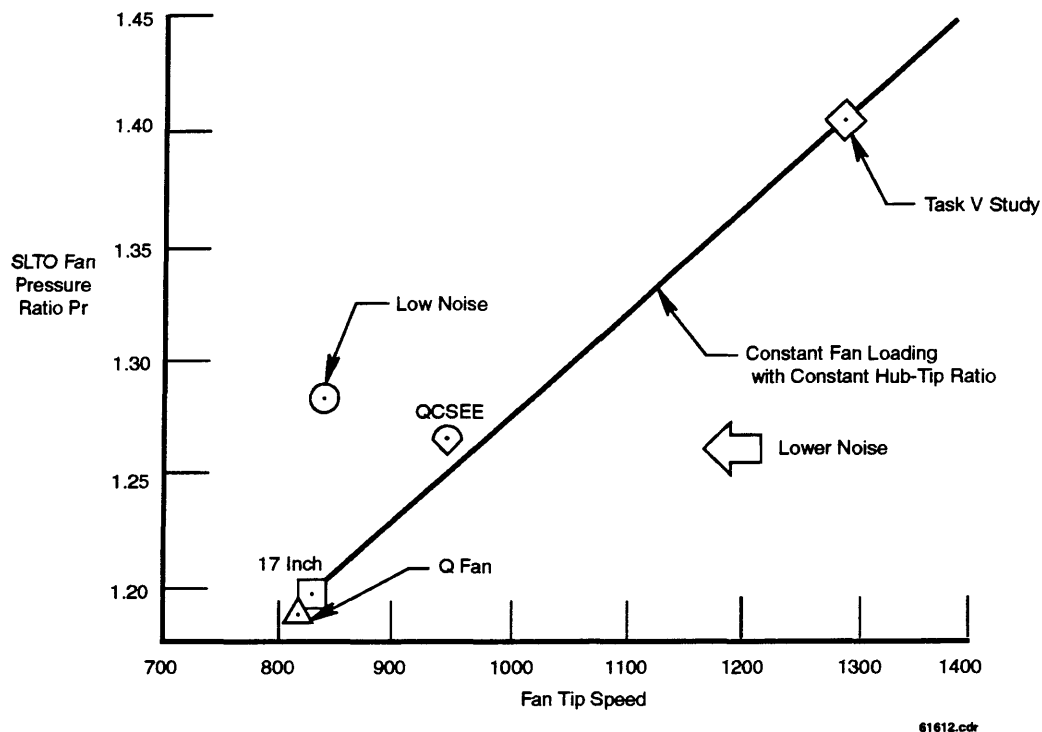
Figure 2-1. Low Noise Fan Stage Design

TASK2FR2.DOC
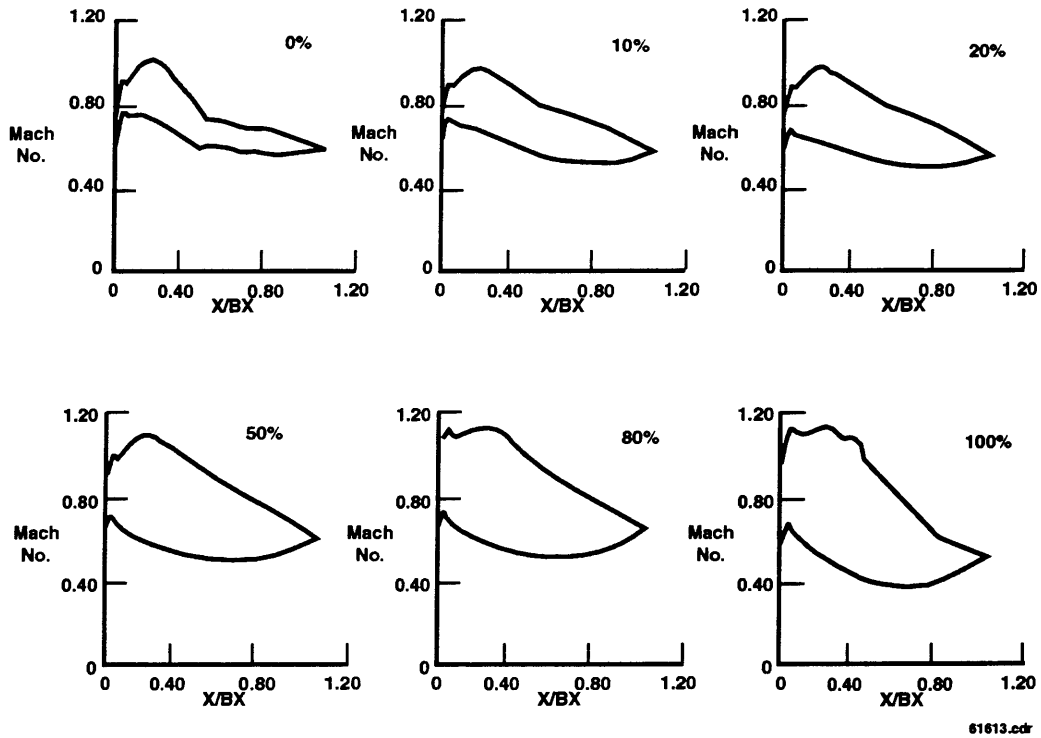
Figure 2-2. Low Noise Fan Stage Design: Fan Mach Distributions, Separation Free at All Spans

SLTO

Max. Flow
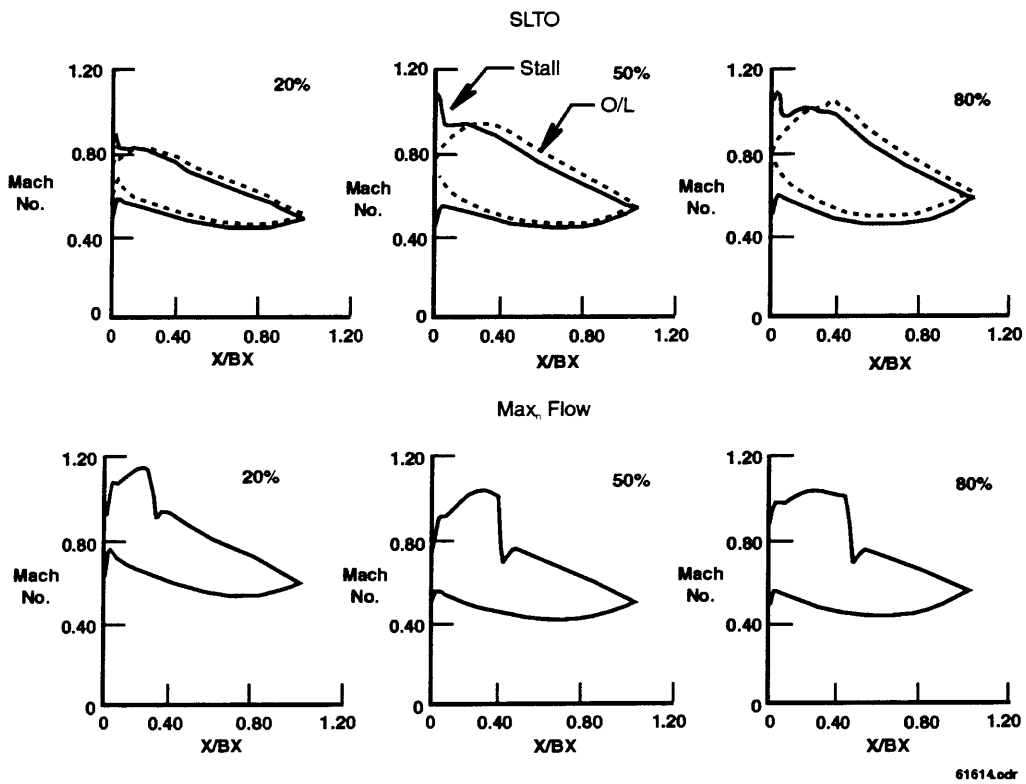
Figure 2-3. Low Noise Fan Off-Design Mach Contours, SLTO

7

Suction Surface   Top Views
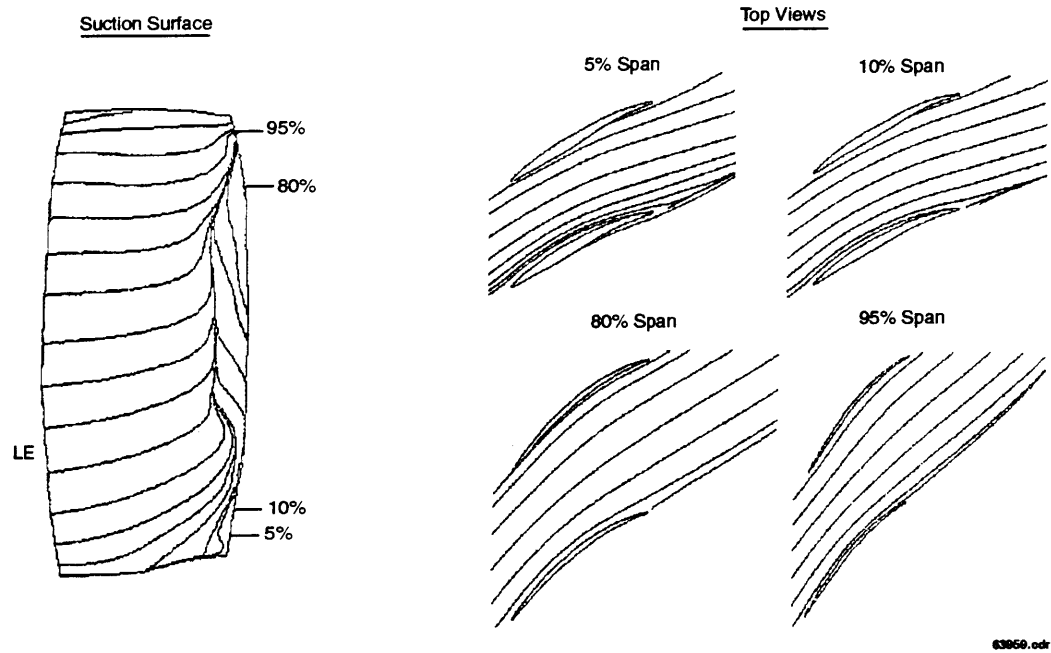
*Figure 2-4. Low Noise Fan Design: Navier-Stokes Streaklines at Cruise,
No Separation Indicated*

Suction Surface   Top Views
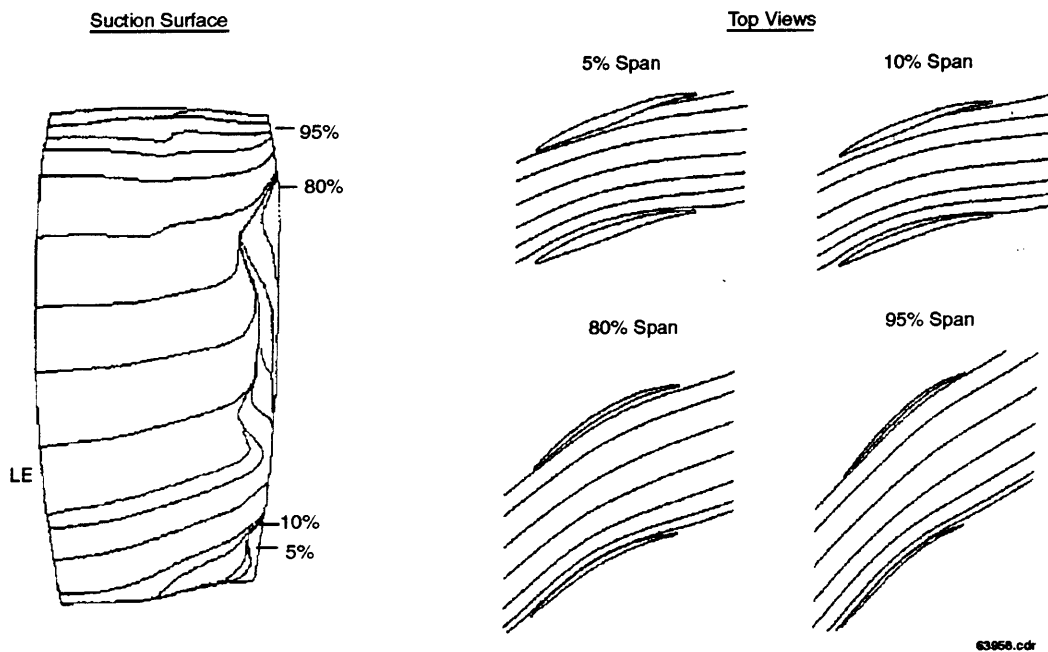
*Figure 2-5. Low Noise Fan Design: Navier-Stokes Streaklines at SLTO,
No Separation Indicated*
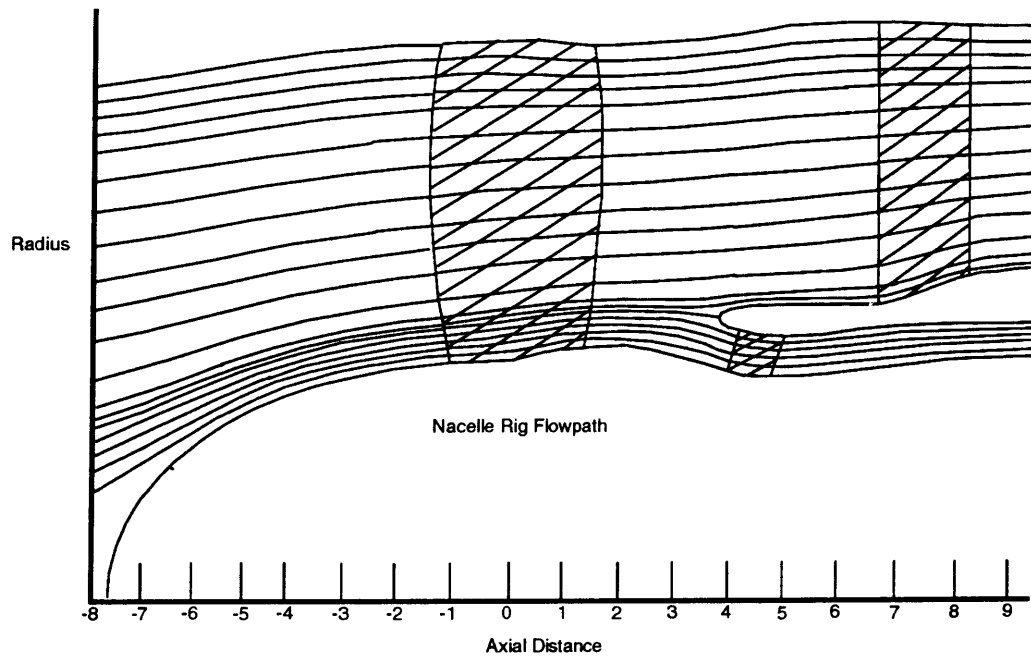
Figure 2-6. Low Noise Fan Design
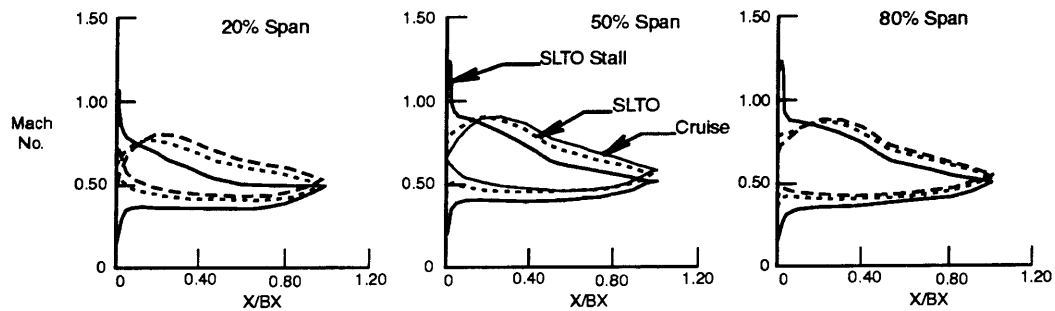
Figure 2-7. Low Noise Fan Design; Nacelle Rig FEGV Stall Incidence Mach Contours

9
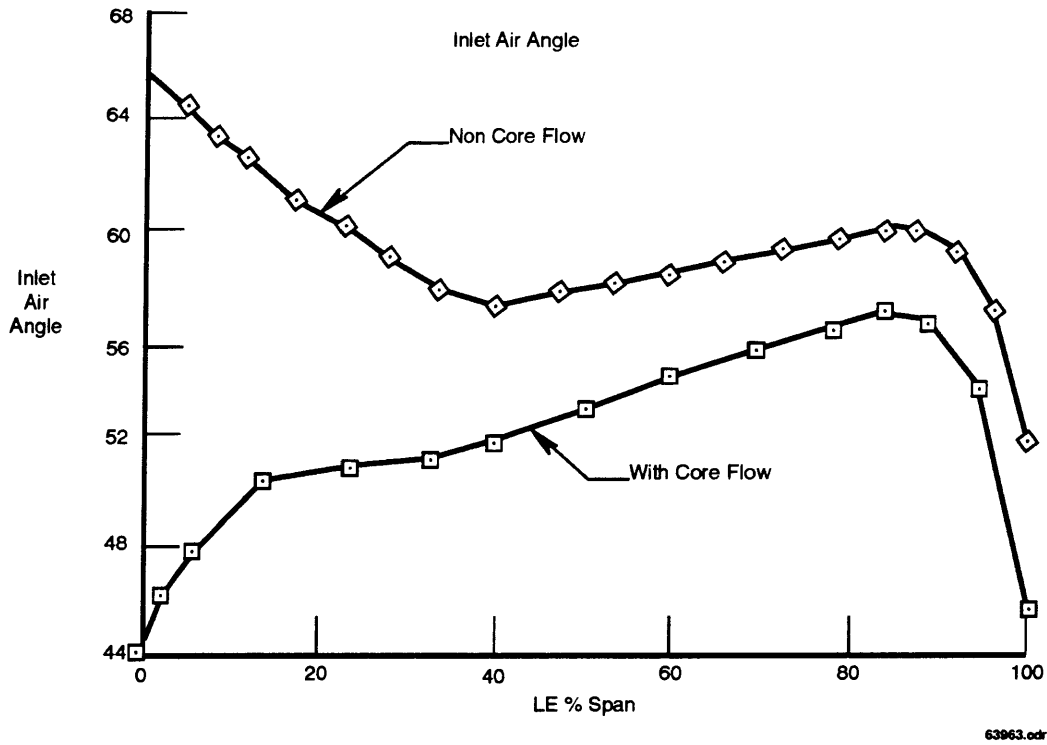
Figure 2-8. Low Noise FEGV at Cruise
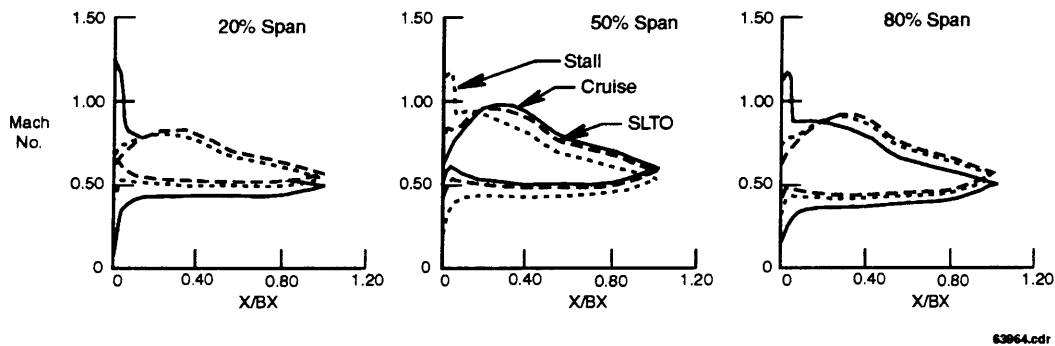
Figure 2-9. Low Noise Fan Design; Non-Core Flow FEGV Stall Incidence Mach Contours

10
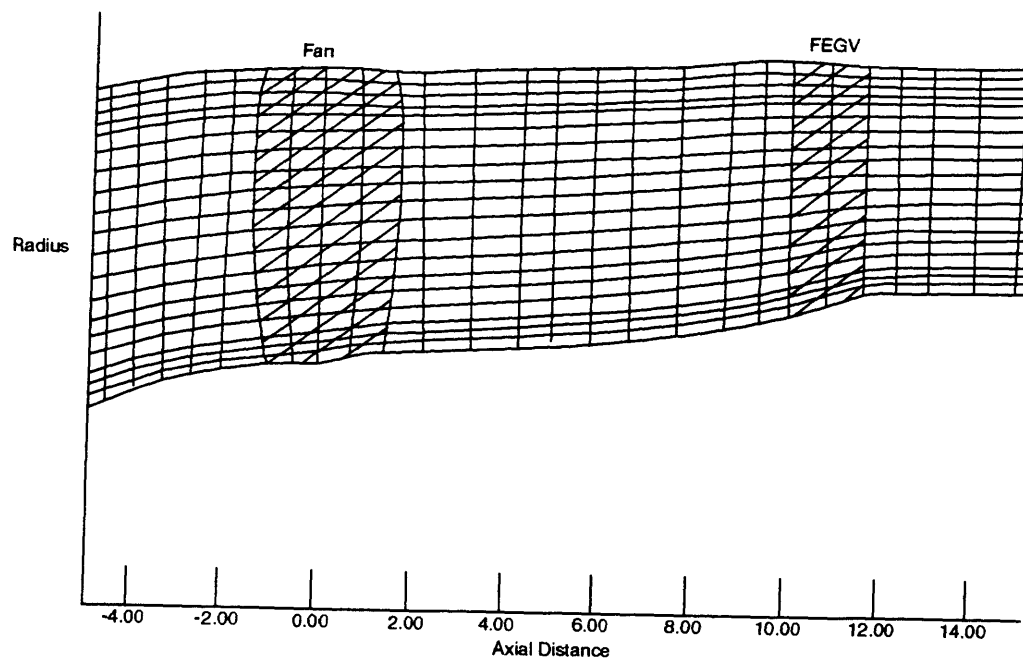
Figure 2-10. Low Noise Fan Design; Non-Core Flow Configuration

3. FAN STRUCTURAL DESIGN

3.1 Objective

The low noise model fan blade was structurally designed to be consistent with the model test requirements. The model blade features a titanium spar/composite shell construction with an integral hub platform. This section summarizes material selections and the analysis performed to determine areas of stress, deflection, resonance frequencies, and flutter. NASA Lewis Research Center (LeRC) participated in the structural analysis and will fabricate the spar/shell fan blades.

3.2 Material Selection

The geometric parameters, rotational speeds, and aerodynamic conditions used in the material selection and structural analyses are summarized in Table 3-1.

Table 3-1. General Airfoil Information

Material	Spar: AMS4928 Shell: 2148A1B carbon fiber
Blade Count	18
Fan Pressure Ratio at Design Point	1.29
Flow Rate at Design Point ($lb_m ft^2$/sec)	91.2
Design Point $N1_{mech}$ (rpm)	8397
Redline $N1_{mech}$ (rpm)	10536
Hot Day SLTO $N1_{mech}$ (rpm)	8750
Minimum Cruise $N1_{mech}$ (rpm)	8100
Flight Idle $N1_{mech}$ (rpm)	5229
Redline Average Tip Speed (ft/sec)	1040
Average Root Radius (in.)	4.83
Average Tip Radius (in.)	11.00
Standard Day Temperature	59°F
Hot Day Temperature	(standard day +27°F)

Three materials are used in the airfoil and attachment assembly. The spar/integral platform and receiver are made from PWA 1228 titanium. Titanium was selected to minimize the centrifugal pull loads on the attachment system. The pins are made from high strength steel, AerMet 100. Bending and shear loads were high enough in the pin to require a high strength steel to obtain adequate safety margin. Airfoil shells are made from carbon epoxy unidirectional tape. HYE 2148A1B tape was selected as the airfoil shell material. Table 3-2 lists the mechanical properties of HYE 2148A1B. This shell material was chosen based on NASA LeRC's good experience and the high elastic modulus needed for this design.

Table 3-2. HYE 2148A1B Carbon/Epoxy Material Properties

Parameter	Symbol	Value
Fiber Volume Ratio	V_{fr}	0.60
Density	ρ	0.056 lb/in^3
Longitudinal Modulus	E_{xx}	34.68E6 psi
Transverse Modulus	E_{yy}	0.96E6 psi
Poisson's Ratio	n_{xy}	0.300
Shear Modulus	G_{xy}	0.62E6 psi
Transverse Shear Moduli	G_{xz}, G_{yz}	0.62E6 psi
Longitudinal Tensile Strength	X_t	175.7.0E3 psi
Longitudinal Compressive Strength	X_c	175.7.0E3 psi
Transverse Tensile Strength	Y_t	5.0E3 psi
Transverse Compressive Strength	Y_c	15.0E3 psi
Interlaminar Shear Strength	S	9.3E3 psi
Cured Layer Thickness (Tensile Specimen)	t	0.0034 in.
Cured Layer Thickness (Shear Specimen)	t	0.0033 in.

Source: properties supplied by Fiberite to NASA LeRC

3.3 Blade Attachment Sizing and Steady Stress

Attachment sizing was performed using the U.S. Air Force Lug Analysis.[3] Attachment nominal stresses were calculated at redline to insure that material yielding occurs locally in stress concentration areas. All life calculations were made at the low cycle fatigue (LCF) rotor speed which is a more typical operating condition than redline. The LCF rotor speed is a combination of the hot day maximum climb rotor speed plus two hundred rpm for wind tunnel rotor speed controller overshoot. This results in an LCF speed of 9867 rpm (mechanical).

Two assumptions were made in sizing the attachment related to pin stress limits and blade tang load split. Pin stresses were limited to levels less than the material yield stress. Easier attachment disassembly is ensured, since no plastic deformation of the pin will occur. Centrifugal pull loads were split according to the U.S. Air Force Lug Analysis section on multiple tang assemblies. As a result, the load split for the blade tangs is 21 percent for each outer end tang and 58 percent for the center tang. Attachment nominal steady stresses at the redline rotor speed are summarized in Table 3-3. These are acceptable with adequate factors of safety.

Acceptable LCF life is predicted for all attachment concentrated stress areas. The maximum number of LCF cycles was selected using a NASA LeRC guideline, three times the number of estimated rig startup-shutdown cycles. This maximum was estimated at 1000 cycles. Acceptable LCF lives require peening of the concentrated stress locations. These locations are inside the pin holes of each tang. Table 3-4 summarizes the concentrated stresses and respective stage lives. The peak stress locations on the receiver tangs and blade tangs occur in the hole.

---

[3] U.S. Air Force Flight Dynamics Laboratory Technical Report, AFFDL-TR-69-V2, February, 1970.

Table 3-3. Attachment Redline Nominal Steady Stresses

	Stress (ksi)	Stress Allowable (ksi)	Safety Factor
Retention Pin Steel			
• Bending	83.8	220.0	2.63
• Shear	37.4	121.0	3.24
Blade End Tangs (Titanium)			
• Tear Out	22.8	59.0	2.59
• Membrane (top of tang)	14.5	108.0	7.44
• Membrane (pin hole)	29.0	108.0	3.72
• Contact	147.2	162.0	1.10
• Bearing Surface	31.7	65.0	2.05
Blade Middle Tang (Titanium)			
• Tear Out	28.2	59.0	2.09
• Membrane (top of tang)	18.0	108.0	6.00
• Membrane (pin hole)	35.9	108.0	3.01
• Contact	147.2	162.0	1.10
• Bearing Surface	39.2	65.0	1.65
Receiver Tangs (Titanium)			
• Tear Out	30.8	59.0	1.92
• Membrane (top of tang)	15.1	108.0	7.15
• Membrane (pin hole)	24.5	108.0	4.41
• Contact	120.7	162.0	1.34
• Bearing Surface	42.8	65.0	1.52

Table 3-4. Attachment Concentrated Steady Stresses

Attachment Component	Stress (ksi)	Blade Life (cycle)	Stage Life (cycle)
End Blade Tangs	110.1	75,000	44,900
Middle Blade Tang	136.3	9500	5700
Receiver Tangs	95.6	$>10^5$	$>30,000$
Receiver Circular Dovetail	39.1	$>10^5$	$>30,000$

3.4 Blade Spar/Shell Interface Stress

Minimum spar bond area was defined from NASA LeRC pull test data of a similarly constructed blade. Twenty specimens were tested. Data ranged from 8300 to 12,000 lb of load for a debonding failure. Failure load distribution statistics were not available, so the minimum load was used in setting the spar area. Test specimens had a nominal area of 6.860 in^2. The resulting nominal shear strength is 1,210 psi.

The maximum composite shell redline pull is 2,446 lb for a volume of 1.645 in^3 and a center of gravity radius of 7.969 in. Therefore the minimum spar area required is 2.021 in^2. A safety factor of four results from the available area, 8.260 in^2, divided by the required area.

3.5 Blade Receiver/Spar Pin Springrate

Pin springrates are calculated to determine the boundary conditions between the blade tang hole and the pin. The springrates are due to a centrifugal restoring force inducing a moment about the pin and blade contact point. The stiffness matrix, K, contains the pin translation, rotation, and coupling terms. Springrates are governed by a few attachment geometric parameters and the blade and pin centrifugal pulls at the speed of interest. K_{11} is the translational stiffness normal to the pin's centerline axis. K_{22} is the rotational stiffness about the same axis. K_{12} and K_{21} are coupling terms. The total springrate was divided by the number of tangs to create the NASTRAN finite element CELAS2 cards. These were then applied to each blade tang base. A NASA technical memorandum[4] discusses the method for applying springrates with coupling terms.

$$K = \begin{bmatrix} \dfrac{Fcf}{4DR} + \dfrac{Fcf}{4dR} - \dfrac{Fcfp}{4DR} & -Fcf\dfrac{Rh}{2DR} + Fcfp\dfrac{Rh}{2DR} \\[4mm] -Fcfb\dfrac{Rh}{2DR} & Fcfb\dfrac{RhRp}{DR} \end{bmatrix}$$

Where:

Rh= blade tang hole radius
Rp= pin radius
Rd= disk tang hole
Fcfb= blade centrifugal pull
Fcfp= pin centrifugal pull
Fcf= blade and pin centrifugal pull
dR= Rd-Rp
DR= Rh-Rp

3.6 Airfoil Finite Element Model

The finite element model was generated for the execution of MSC/NASTRAN Version 67.[5] Three element types were used in modeling the airfoil; beams for the attachment, bricks for the spar and plates for the composite shell. A geometric nonlinear analysis, solution 106, is run for static stress and strain results. A combination of solutions 63 and 64 are run to obtain frequencies and mode shapes. Air pressure loads for the aerodynamic design point, sea level takeoff, maximum climb and redline conditions were created as PLOAD2 cards. Model rotations, to represent various angles of attack, are performed in NASTRAN by selecting the coordinate system corresponding to the operating condition.

---

[4] NASA Technical Memorandum 89900, *Hub Flexibility Effects On Propfan Vibration*, Michael A. Ernst and Lawrence, NASA Lewis Researh Center, July, 1987.

[5] MSC/NASTRAN Version 67 User's Manual, Vol 1 & 2, © August, 1991, MacNeal-Schwendler Corporation

3.7 Blade Airfoil Steady Stress

Airfoil steady stress levels were computed at redline with the appropriate air pressure loads. The Hoffman failure criteria was selected to assess the durability of the design. This criteria was selected due to the composite construction, the biaxial state of stress, and the lack of a strength interaction term. This strength interaction term, F_{12}, requires testing of the laminate, which was not available. This interaction term was accordingly set to zero, reducing the Tsai-Wu criteria to the Hoffman criteria.

MSC/NASTRAN computes the Hoffman failure indices internally. Each layer of every element has a failure index calculated. An acceptable design should have a maximum failure index below 1.0. The maximum failure index is 0.455. The peak occurs in the second layer from the concave surface above the trailing edge tang.

3.8 Resonance Vibration and Flutter

Figure 3-1 is a Campbell diagram for the low noise fan. The fan geometry has acceptable frequency characteristics. Reduced velocity parameters are used to determine transonic stall flutter stability. Table 3-5 illustrates that the low noise advanced ducted propulsor fan has acceptable reduced velocity parameters.

Table 3-5. Low Noise Advanced Ducted Propulsor Fan Velocity Parameters

Vibratory Mode	Reduced Velocity Flutter Parameters	Low Noise Fan Reduced Velocities
First Bending	$24V/bw_b$	4.79
First Torsion	$24V/bw_t$	1.74

3.9 Disk Stress and Deflection Analysis

The disk is composed of two halves held together with axially oriented tie bolts. A split disk configuration is required from the fan circular dovetail attachment design. Calculations were made to verify the design satisfies stress, burst margin and LCF requirements. Deflections were computed to examine axial separation of the disk halves and radial growth.

AMS5659 stainless steel is used as the disk material. Material properties are summarized in Table 3-6. Low cycle fatigue data is plotted in Figure 3-2 as nominal stress versus cycles to crack initiation for AMS5643. Use of this data is acceptable since the delta ferrites, which affect transverse strength in the AMS5643 microstructure, are minimized in AMS5659.

A three-dimensional GPBEST boundary element mode was generated in Patran 3.0.[6][7] A one-thirty sixth slice of the disk is modeled. Roller type boundary conditions are placed on the symmetry planes. Tie bolt preload, tie bolt centrifugal load, and airfoil centrifugal load are applied as surface tractions. Disk body forces are applied through centrifugal loading. A nonlinear static analysis, with contact between the disk halves, is run to obtain stresses and deflections. A frictionless surface is assumed at the disk half interface.

Satisfactory burst margin is predicted for this disk design.[8] Appendix C summarizes the average tangential stress calculations. The resulting average tangential stress of 29.6 ksi is less than the allowable tangential stress of 70.0 ksi.

---

[6] Patran 3 User's Manual, Release 1.1B, June, 1993, PDA Engineering, Costa Mesa, CA.

[7] GPBEST User's Manual, Version 4.2, April, 1993, BESTC, Getzville, NY.

[8] NASA 8 ft x 6 ft Supersonic Wind Tunnel User Manual, Ronald H. Soeder, Lewis Research Center, Cleveland OH, February, 1993.

Acceptable LCF, 50,000 cycles, is predicted for all concentrated stress areas. The minimum number of LCF cycles was selected using a NASA LeRC guideline: three times the number of estimated rig cycles. This minimum was estimated at 1000 cycles. All life calculations were made at the LCF rotor speed, which is a more typical operating condition than redline. The rotor speed is a combination of the hot day maximum climb rotor speed plus two hundred rpm for rotor speed controller overshoot. This results in an LCF speed of 9878 rpm (mechanical).

Peak stresses occur in the receiver and tie bolt holes at 70.0 ksi each. The stress concentration factor at these locations was calculated by dividing the LCF speed average tangential stress into the peak stress. A K_t of 2.85 results. This was rounded up to 3.0 for conservatism.

Redline deflections were computed to examine the radial and axial growths. Axial deflections were examined to verify the tie bolt preload prevents disk half separation. Due to the different radial heights of the halves, radial growths were examined to insure growth differences were small. Only 1.9 mils of radial growth difference is predicted along the frictionless split line. This is considered acceptable. Actual growth differences will be smaller since friction is present.

Table 3-6. AMS 5659 Material Properties at 150°F

Parameter	Symbol	Value
Elastic Modulus	E	$29.5E6 \text{ lb/in}^2$
Poisson's Ratio	ν	0.272
Density	ρ	0.283 lb/in^3
Ultimate Tensile Strength	σ_{UTS}	$150.0E3 \text{ lb/in}^2$
Yield Strength	σ_{YS}	$140.0E3 \text{ lb/in}^2$

3.10 Tierod Design and Stress Analysis

The two disk halves are clamped together axially with 18 tierods made of Inconel 718 nickel alloy and double hex Waspalloy nuts. Cold static preload for the composite blade will be a maximum of 15,800 pounds or approximately 800 lb-in of torque. To ensure this preload will be achieved, but not exceeded, tierod stretch will be measured during assembly. This preload ensures the two disk halves will not roll apart due to the blade centrifugal pull imparted into the disk through the 45-degree cone seat.

The above preload is based on an ultimate tensile strength of 220,000 psi and the area at the minimum thread diameter. This tensile stress area is defined in National Bureau of Standards Handbook H28.

Parameter	Value
Ultimate Strength	26.0E3 psi
Safety Factor	1.250
Proof Strength	20.8E3 psi
NASA Specified 90 Percent Limit Strength	18.72E3 psi
Maximum Preload	15.8E3 lb (76 percent of proof)
Minimum Preload	13.55E3 lb (65 percent of proof)

Tierod bending stress will exist at the disk parting planes, due to the uneven radial shift of the two disk halves. However, this stress is only 54 percent of proof strength, because of the increased diameter of the tierod shank.

3.11 Tierod Nut Design and Stress Analysis

The self-locking nuts are AMS5709 Waspalloy material. A vonMises equivalent stress was calculated for the thread accounting for radial pressure, hoop stress, compressive stress in the collar portion, and shear. This principle stress, under worst condition, is at 82 percent of 98,000 psi yield strength.
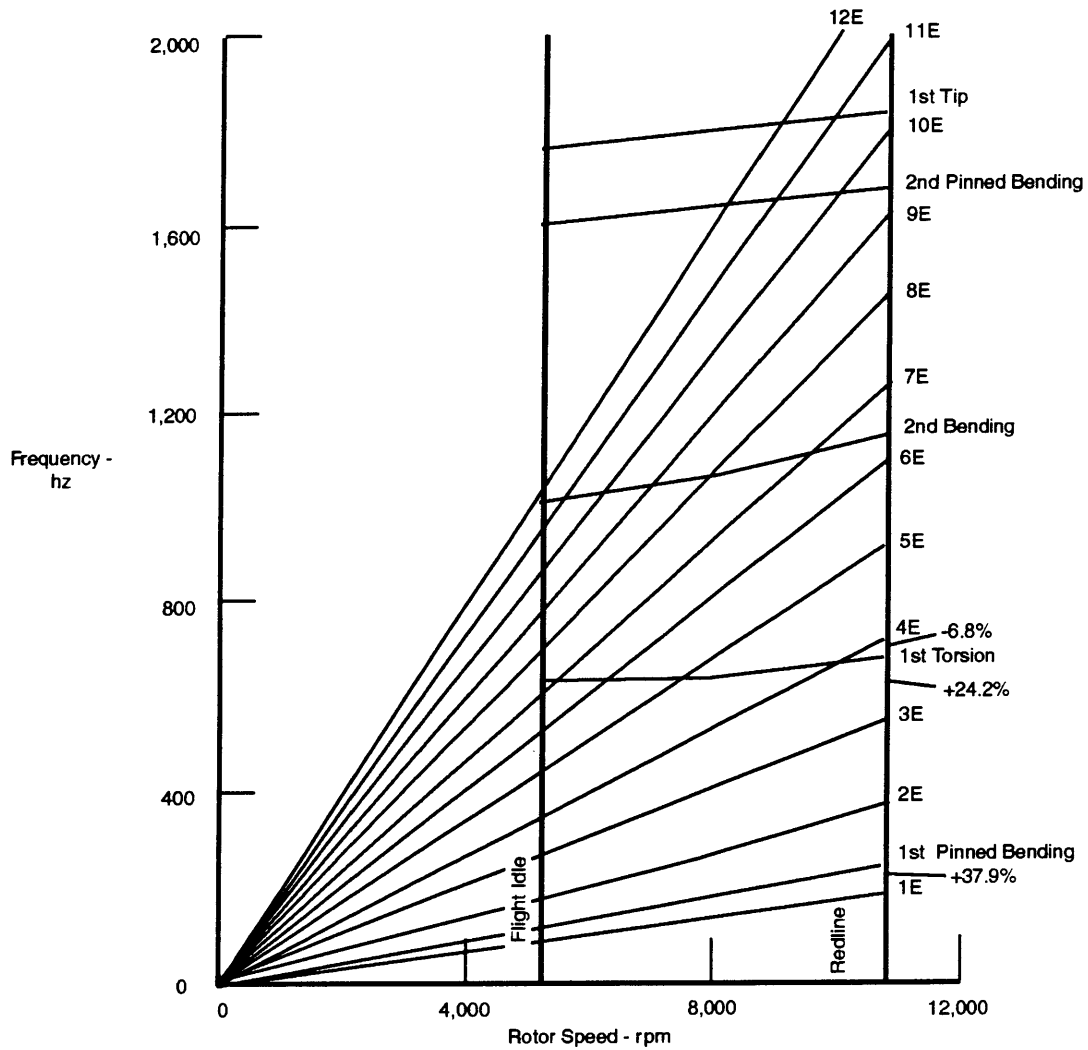
Figure 3-1. Low Noise Composite Pinroot Fan Revision 9 Geometry Campbell Diagram

19

AMS 5643(H1025) Minimum Low Cycle Fatigue Data
200 °F, R = 0 (Zero Minimum Stress)

Normal Stress

Kt = 1.0

Kt = 3.0

Cycles

63967.cdr

Figure 3-2. AMS5643 (H1025) Minimum Low Cycle Fatigue Data

20

4. FAN STAGE ACOUSTIC DESIGN

4.1 Objective

The objective of this task was to determine the fan blade/fan exit guide vane (FEGV) number ratio which would minimize fan tone noise. The number of blades was fixed at 18 and the vane number was then chosen to minimize the fan noise. The analysis used for the blade/vane optimization was the recently updated version of the Fan Noise Prediction Code[9,10,11]. This theoretical model predicts the inlet and aft propagating fan tone power levels due to the interaction of fan wakes with the FEGVs and the compressor inlet guide vanes. In the current study, this code was used to make fan tone noise predictions for 18 blades and vane counts ranging from 11 to 85. Predictions were performed over the entire speed range of interest (sideline, takeoff, cutback, and approach). Predicted tone deltas were applied to typical engine measured data to assess the total engine noise levels at the different blade/vane combinations. Based on this study, a configuration of 45 vanes with 18 blades was predicted to result in minimum noise. This vane number was chosen to cutoff blade passage frequency (BPF) and has been optimized for the higher harmonics, 2BPF and 3BPF.

4.2 Fan Tone Noise Prediction System

One of the major sources of fan tone noise in a turbofan engine is the interaction of the fan rotor wakes with the downstream stator vanes. The wakes result in an unsteady velocity fie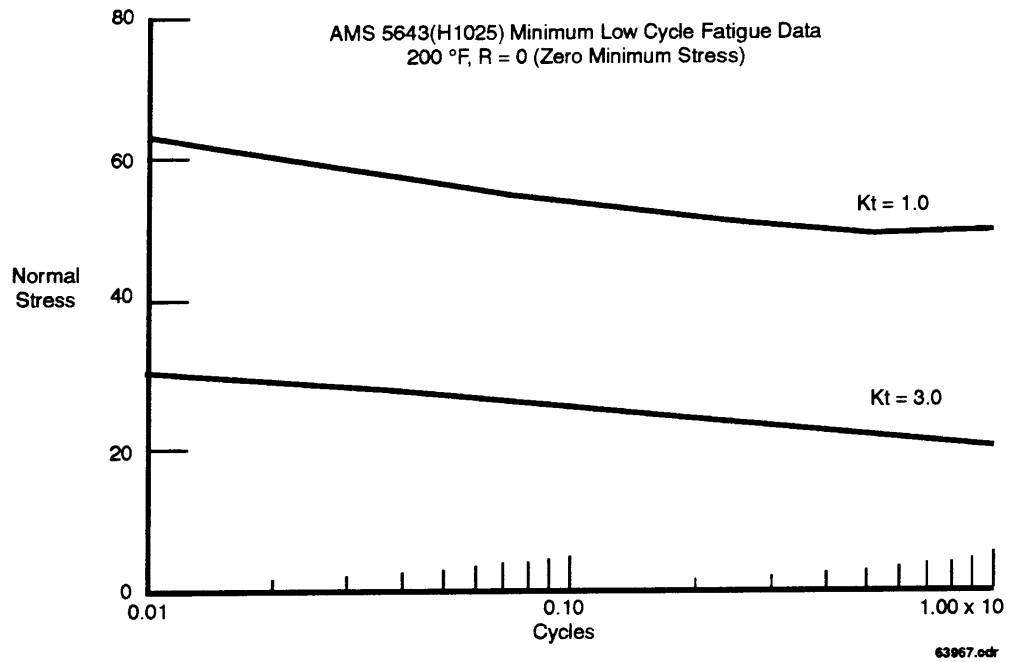ld which is convected downstream into the stators. As a result, the stators experience unsteady lift forces and respond by radiating pressure fields. The pressure waves of adjacent stators merge and may propagate in the engine duct and then to the far field. Therefore, the tone noise emitted at the BPF and its higher harmonics is directly related to the unsteady flow field generated by the wakes of the fan blades.

Fan noise analysis predicts the tone power levels due to rotor-stator interaction. However, this is just one of the many noise components which contribute to the total engine noise. A design which reduces the tone levels may not effect the total noise if other components are significantly higher than the tone noise. As a result, a set of representative data must be used to assess the importance of the fan tones relative to the other noise sources.

Subsequent to the completion of this study and report, the fan tone noise prediction system was incorporated into a more comprehensive fan noise prediction system. During this work, it was discovered that there was an error in the code. Since then, the code has been corrected and improved. There has been no attempt to redo the work covered by this report. If the improved version of the code were used to try to duplicate the results in this study, the predictions would probably be different.

4.3 Engine Sensitivity Study

To determine which tones contribute most significantly to the total noise, a tone noise sensitivity study was performed. The first step of this process required separating the fan tones from the rest of the broadband data. With the tones isolated, each tone was individually reduced and the new tone matrix was recombined with the original broadband data to determine the effect of reducing the tone on the total engine noise. The noise unit chosen for comparison is the PNLTi, which is a PNLT integrated over a specified far field angle

[9] Topol, D.A., *Rotor Wake/Stator Interaction Noise - Predictions vs. Data*, Journal of Aircraft, Vol. 30, No. 5, Sept-Oct. 1993, pp 728-735.

[10] Philbrick, D.A. and D.A. Topol, *Development of a Fan Noise Design System, Part 1: System Design and Source Modeling*, AIAA-93-4415, Oct. 1993.

[11] Topol, D.A., *Development of a Fan Noise Design System, Part 2: Far-Field Radiation and System Evaluation*, AIAA-93-4416, Oct. 1993.

range. The PNLTi's were calculated for both the inlet and aft with the inlet angle range from 10 to 80 degrees, and the aft range from 90 to 150 degrees. Figure 4-1 illustrates the tone sensitivity of engine data at the cutback noise certification condition. This figure illustrates that, individually reduced, the inlet tones do not significantly reduce the total engine noise. Reduction of 2BPF-aft is the only change which would significantly affect the total engine noise at the cutback condition. Similar sensitivity studies were performed at the approach and sideline certification conditions, and the results also indicate that the inlet tones do not significantly contribute to the total noise, and 2BPF-aft does contribute. As a result of this sensitivity study, a vane/blade ratio would be chosen to minimize the 2BPF-aft tone.

4.4 Low Noise Fan Tone Noise Prediction

The fan tone noise prediction analysis was used to predict the duct tone power levels of the fundamental frequency and the first two harmonics for vane counts ranging from 11 to 85. Figure 4-2 illustrates the tone power levels predictions as a function of vane number for BPF, 2BPF, and 3BPF (inlet and aft) at the sideline noise certification condition. Each harmonic has peaks and valleys where the tone noise is maximum or minimum. Figure 4-2a and Figure 4-2b illustrate that BPF inlet and aft will be cutoff for any configuration with more than 32 vanes. 2BPF will be cutoff for configurations with more than 64 vanes. Based on the previous discussion, 2BPF is the tone which contributes significantly to the total engine noise. Figure 4-2d illustrates that a significant reduction would result in 2BPF aft by choosing 32 vanes or anything above 64 vanes (2BPF will be cutoff). However, the changes which occur at the other noise harmonics must be evaluated. For example, by choosing 32 vanes, 2 BPF-inlet and 3BPF-inlet will increase, which is illustrated in Figure 4-2c and Figure 4-2e. Figure 4-3 and Figure 4-4 illustrate similar plots for the cutback and sideline condition.

A blade/vane ratio which minimizes 2BPF-aft cannot simply be chosen without assessing the effect of changes the other tones have on the total noise. As a result, predicted tone deltas relative to the baseline configuration (18 blades, 45 vanes) were calculated for configurations with vane counts ranging from 11 to 85. These tone delta matrices were calculated for the sideline, cutback, and approach conditions using Figure 4-2, Figure 4-3, and Figure 4-4, respectively. These tone deltas were applied to the source separated tone matrix of engine data to simulate the tone noise at all vane numbers between 11 and 85. Because the predicted tone deltas are duct power levels and not far field directivity, it is assumed that the predicted deltas are constant over the inlet or aft angle range. The adjusted tone matrices were then combined with the original separated broadband data to calculate the total noise at each of the vane numbers from 11 to 85. The result is the new total noise due to the effect of changes in the noise harmonics, which are due to vane number changes. This procedure was repeated for all three noise certification conditions: approach, cutback, and sideline.

Figure 4-5a illustrates the change in total noise as a function of vane number for the sideline noise certification condition. The minimum occurs at 46 vanes, unless a vane number above 86 is chosen, which will cutoff BPF, 2BPF, and 3BPF. Figure 4-5b and Figure 4-5c illustrate similar plots for the cutback and approach conditions, respectively. These figures do not include data below 30 vanes because this will result in cuton of BPF, which is not acceptable. In Figure 4-5b (cutback condition), there is a significant rise and then an 8 dB drop in the noise at a configuration of approximately 55 vanes. This is due to the rise of 2BPF-aft just before cutoff, as illustrated in Figure 4-5b. The approach condition, Figure 4-5c, has little variation as a function of vane number, indicating that the tones do not significantly contribute to the total noise.

A very important measure of community noise is the summation of the sideline, cutback, and approach noise conditions. Figure 4-6 illustrates this summation which is the addition of Figure 4-5a, b, and c. There are two minimums on this figure: 44 vanes and 68 vanes. At 44 vanes, the total noise is predicted to be 0.6 dB less than the baseline configuration of 18 blades with 45 vanes. A configuration with 68 vanes would

result in approximately the same noise as the baseline, however, 2BPF would be entirely cut off. This figure illustrates a sharp decrease at 45 vanes due to the cutoff of 2BPF-aft at the cutback condition.

Because the optimum number of vanes is very close to the baseline configuration (18 blades, 45 vanes), the recommended number of vanes is also 45 for the low noise fan model.

4.5 Low Noise Fan-Core Flow Tone Noise Prediction

A simplified but similar study to that described in Section 4.4 was done to predict tone noise from the rotor wake/ core stator interaction. Three numbers of core stator vanes were investigated: 36, 63, and 68. The lowest tone levels at the three noise conditions of sideline, cutback and approach were achieved with 63 core stator vanes.
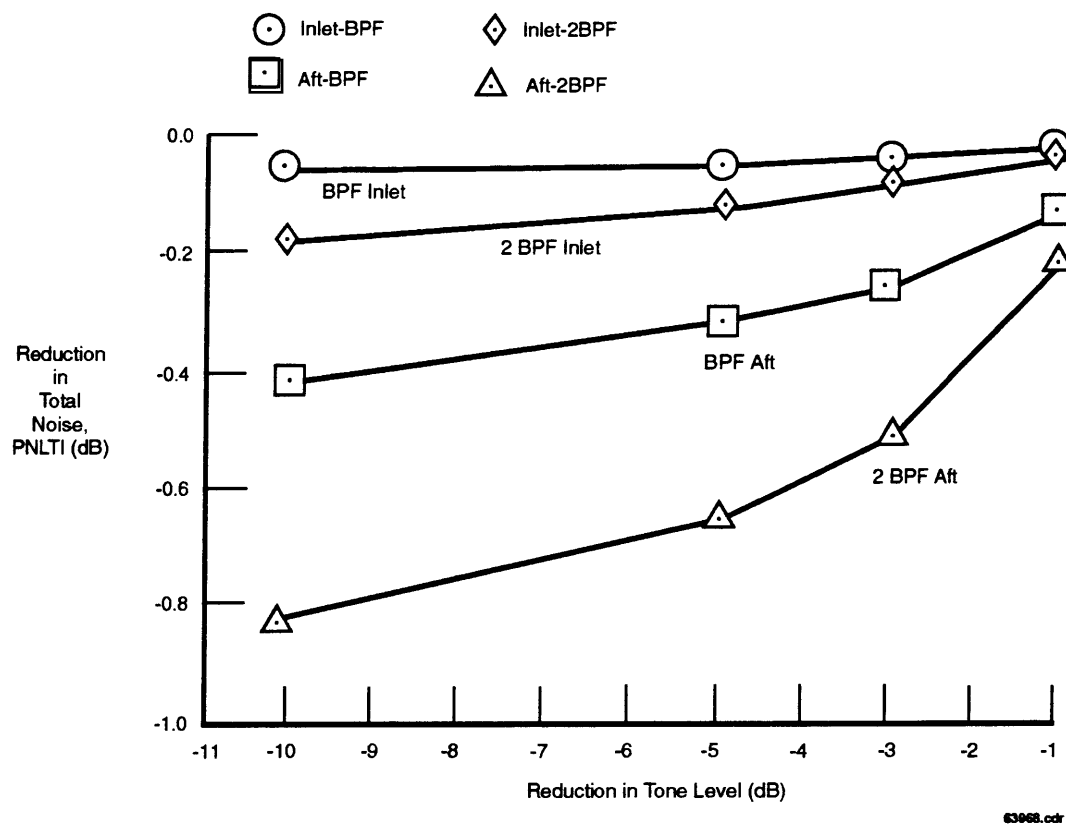
Figure 4-1. Tone Sensitivity of Engine Data At Cutback Noise Certification Condition
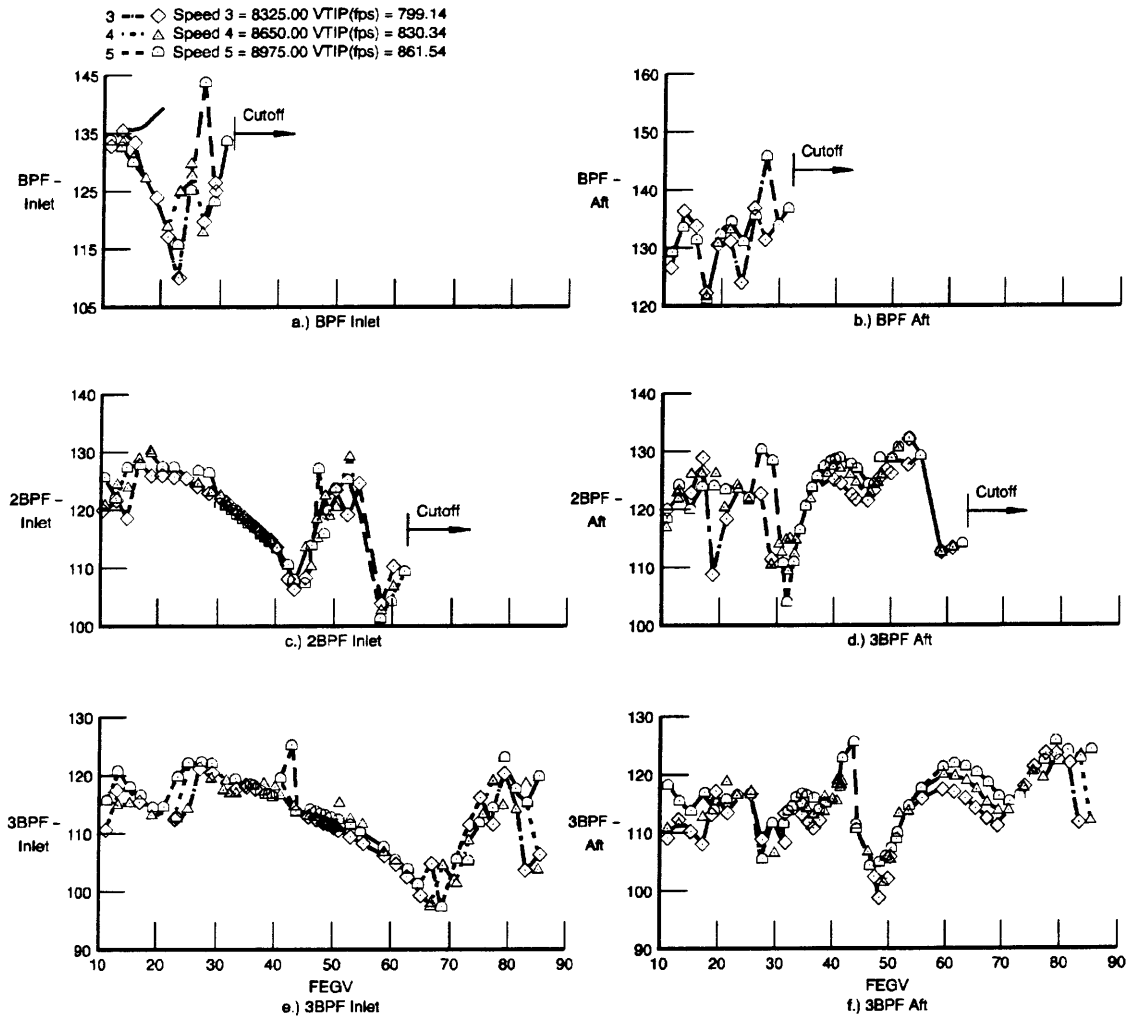
Figure 4-2. Predicted Tone Power Levels for Sideline Noise Certification Condition as a Function of Vane Number
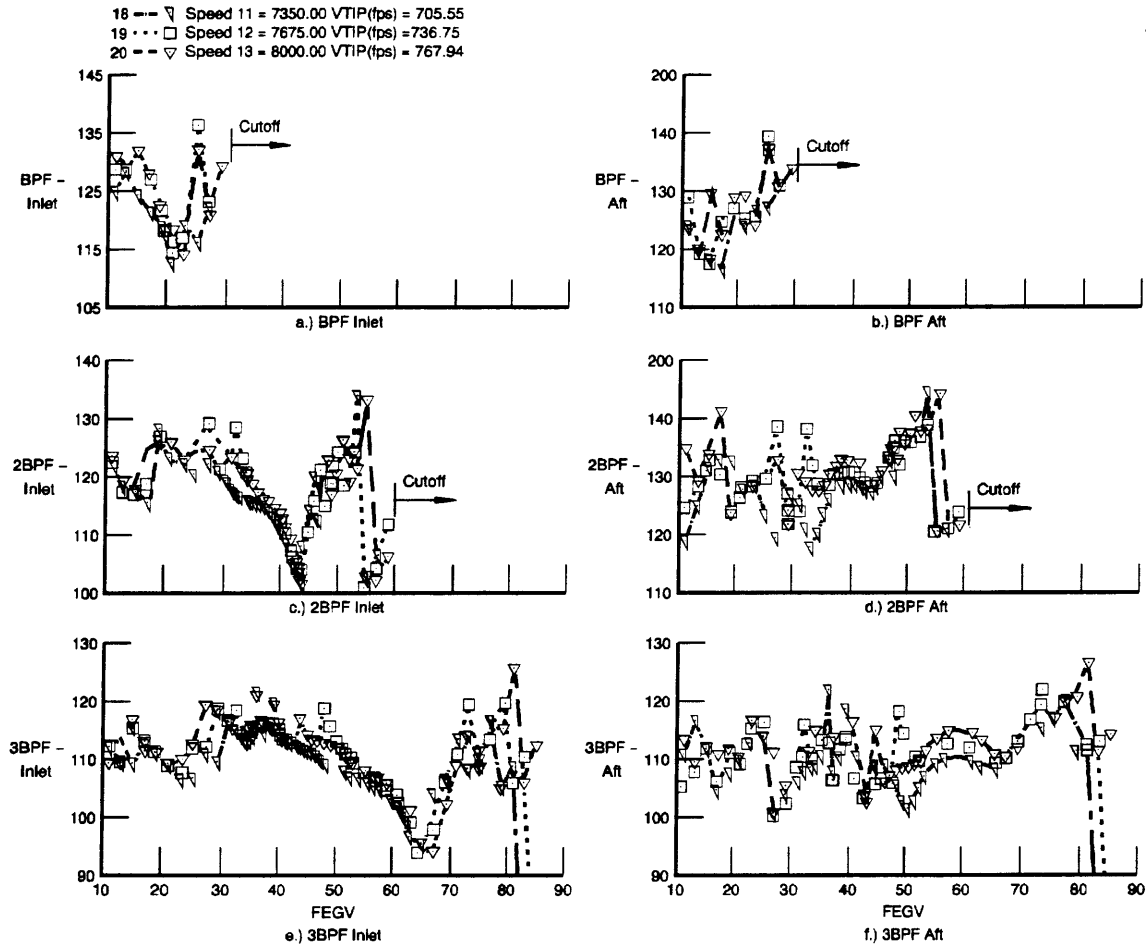
*Figure 4-3. Predicted Tone Power Levels for Cutback Noise Certification Condition
as a Function of Vane Number*
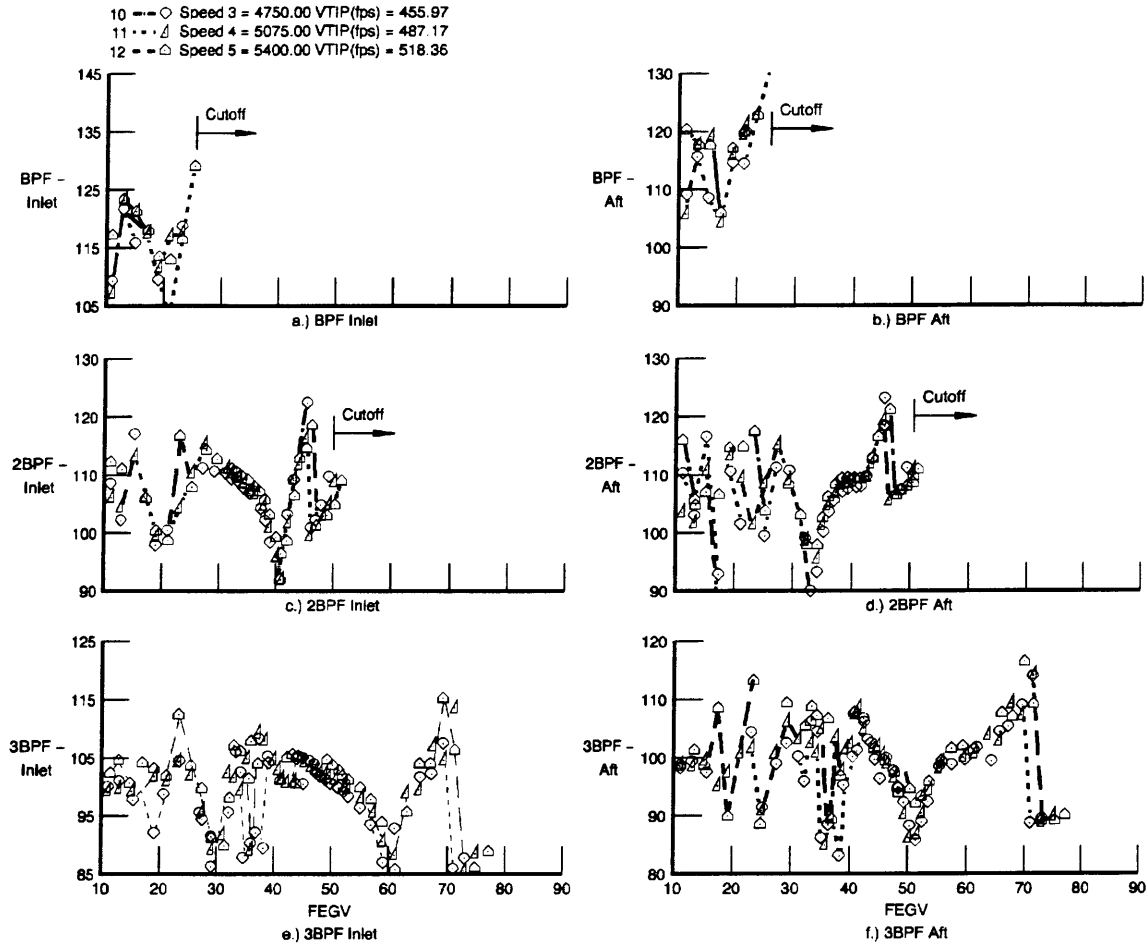
Figure 4-4. Predicted Tone Power Levels for Approach Noise Certification Condition as a Function of Vane Number
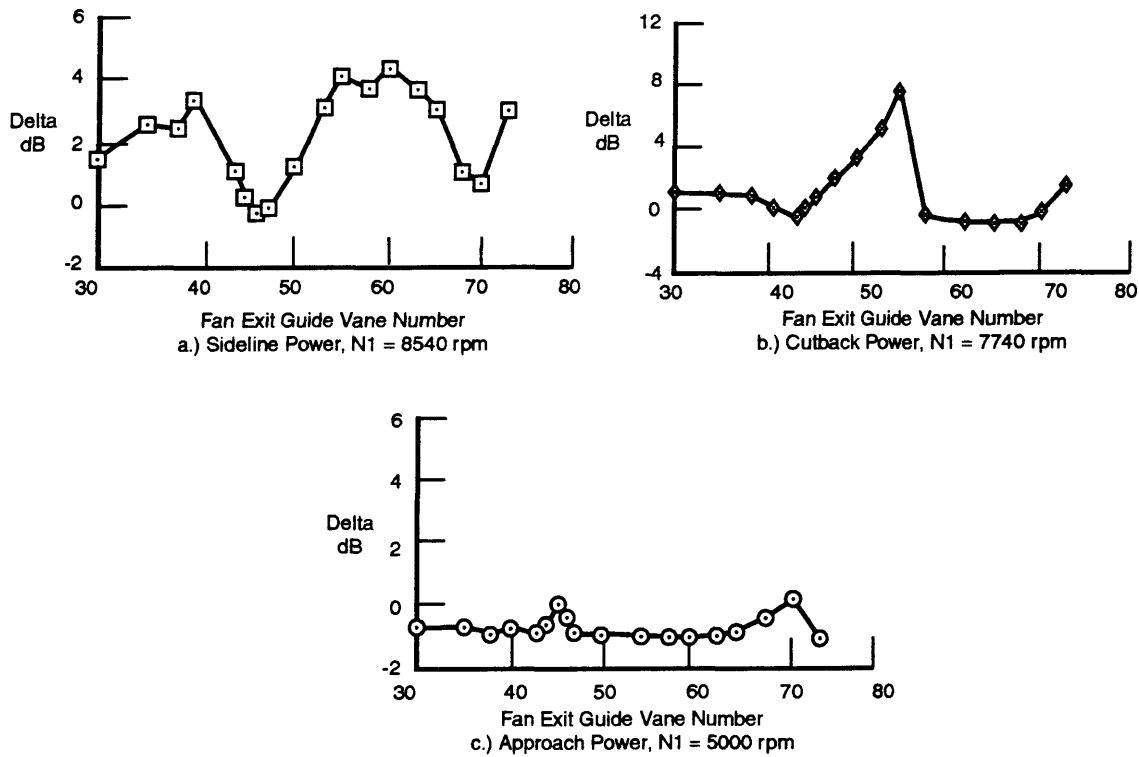
Figure 4-5. Illustration of Total Noise Delta as a Function of Vane Number Relative to Baseline Configuration of 18 Blades, 45 Vanes For Each of the Noise Certification Conditions

28
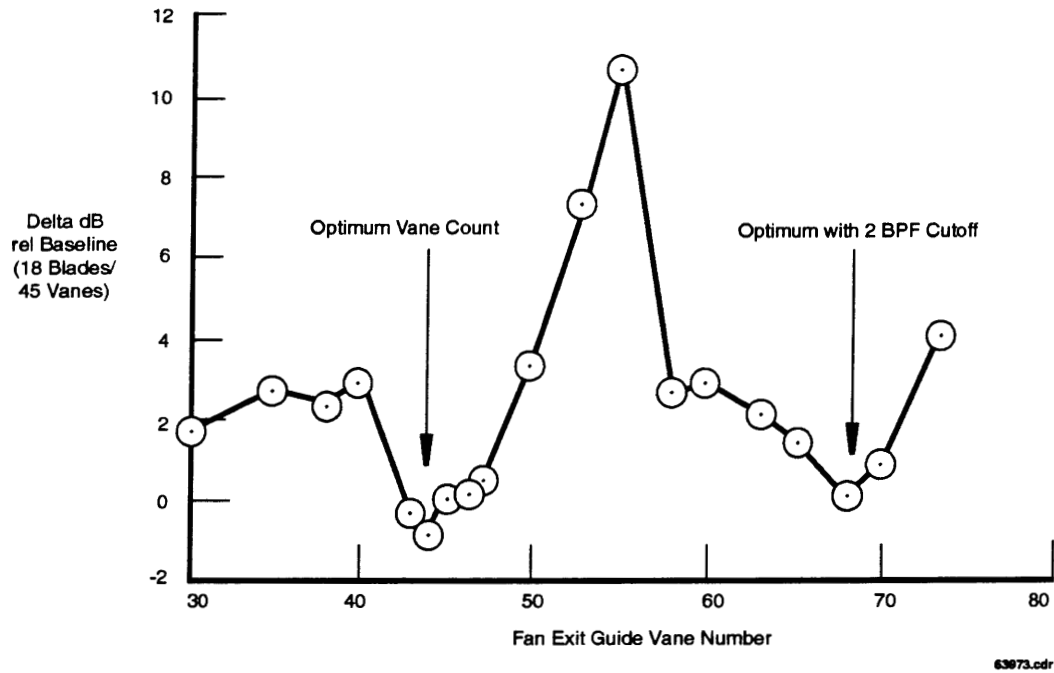
Figure 4-6. Summation of Sideline, Cutback, Approach Noise Configuration Conditions

5. Fan Rotor Navier-Stokes Analysis

5.1 Objective

The objective of the Navier-Stokes analysis was to validate operability of the low noise fan design. A previous similar fan was also analyzed to calibrate the analysis for this type of fan. Figure 5-1 shows the overall fan map comparison of previous fan test results with Navier-Stokes prediction. Stall is predicted quite well. Figure 5-2 shows the fan map comparison of the Low Noise fan Navier-Stokes predicted performance relative to goals. It indicates that Low Noise operability goals are achievable. The analysis also indicates that the fan blade is free of boundary layer separation full span at the cruise design point, Figure 2-4, as well as at takeoff, Figure 2-5.
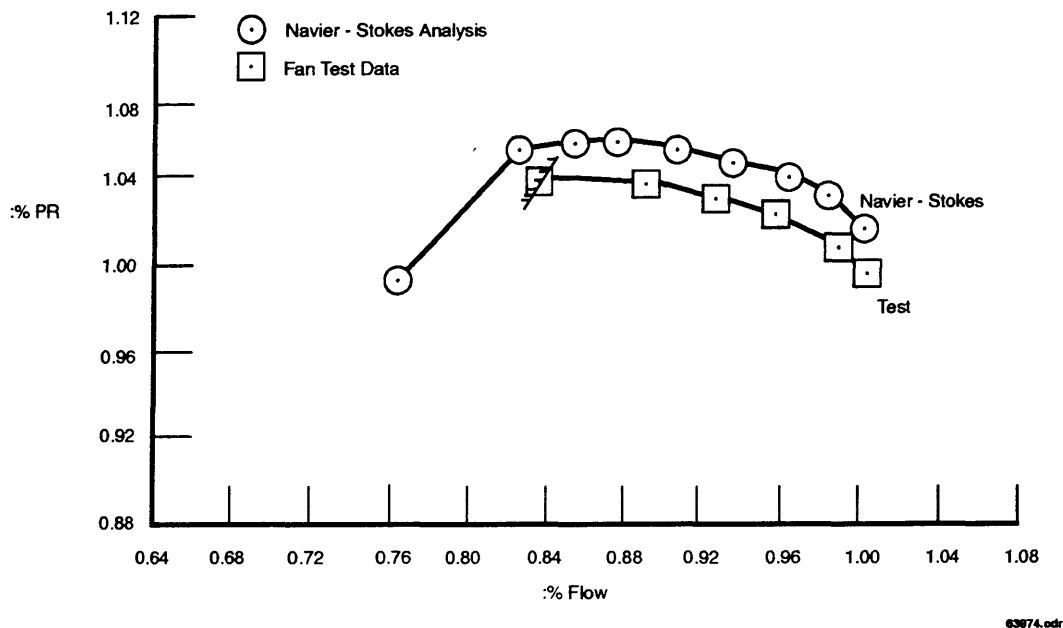
Figure 5-1. Previous P&W Fan Design Comparison of Navier-Stokes to Data With Casing Treatment
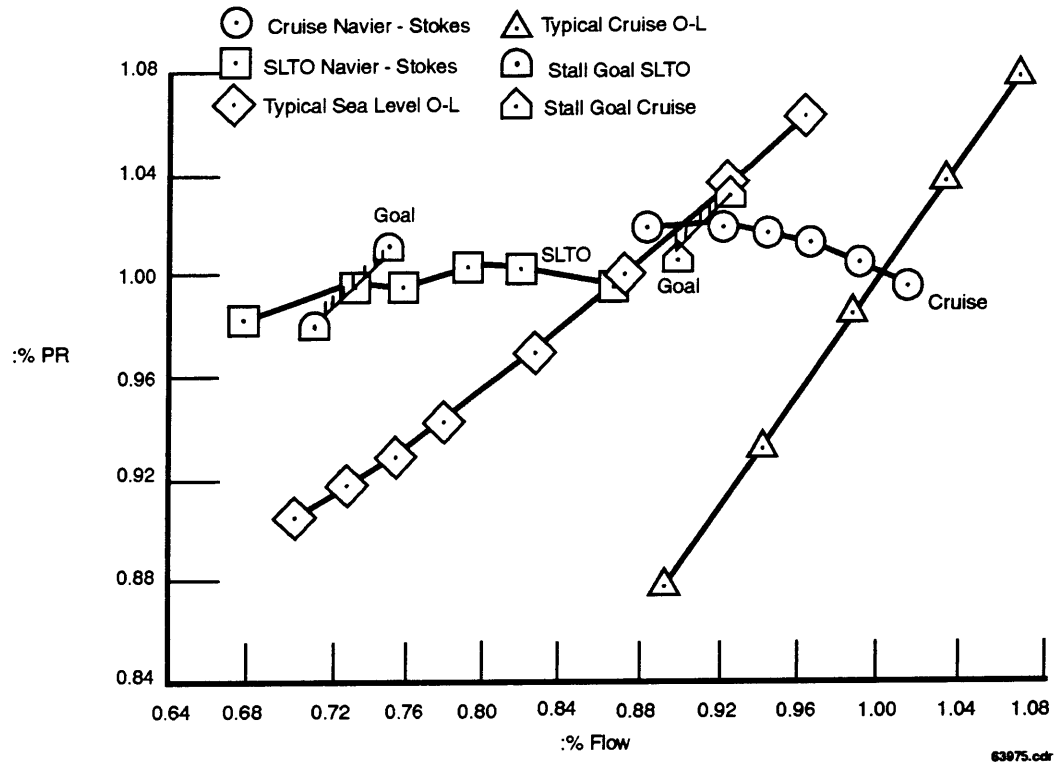
Figure 5-2. Low Noise Fan Design Comparison of Navier-Stokes to Goal

6. NACELLE AERODYNAMIC DESIGN

6.1 Objective

The model nacelle design required was to be typical engine configuration. For ease in testing and fabrication, the nacelle inlet, cowl, and nozzle were all axisymmetric.

6.2 Nacelle Design

The internal fan, hub and tip fan to fan exit guide vane duct and core inlet geometries were supplied from the low noise fan stage design. The nacelle was designed around these boundary conditions using a standard rules based design method. The resulting inlet was found to have acceptable area for acoustic liner; the fan duct was modified to allow full depth treatment to run further aft in the nozzle. The final geometry is shown in Figure 6-1.

6.3 Nacelle Aerodynamic Performance

The inlet was designed to flow without separation or extreme losses at the following operation extremes:

Maximum Flow: The inlet is designed to pass a maximum flow of w = 102.6 lb/sec without any internal shock.

Cruise: The inlet is designed to be shock free with a well-behaved external flowfield at a Mn = 0.82 cruise corrected airflow of 97.23 lb/sec.

Windmill: The inlet is designed to operate without separation at a windmilling corrected airflow of 30.58 lb/sec at 17.9 degree angle of attack (AOA), Mn = 0.27. at 10,000 feet altitude.

Takeoff: The inlet is designed to operate without separation at a takeoff corrected airflow of 85.50 lb/sec at 25 degree AOA, Mn = 0.25 at sea level.

The aerodynamic design and predicted performance was reviewed by NASA and found acceptable for use in the model application. These conditions are summarized in Table 6-1.

Table 6-1. Summary of Inlet Operability Conditions

Case	Mach Number	AOA (degrees)	Pt (psi)	Tt (R)	Flow, w (lb/s)	Alt (ft)	Fan w/A
Cruise	0.82	0	5.3776	446.8	97.23	35,000	45.0
Max Flow	0.82	0	5.3776	446.8	102.62	35,000	47.5
Windmill	0.27	17.9	10.635	490.6	30.58	10,000	14.2
Takeoff	0.25	25	15.375	525.4	85.50	SL	39.6

32
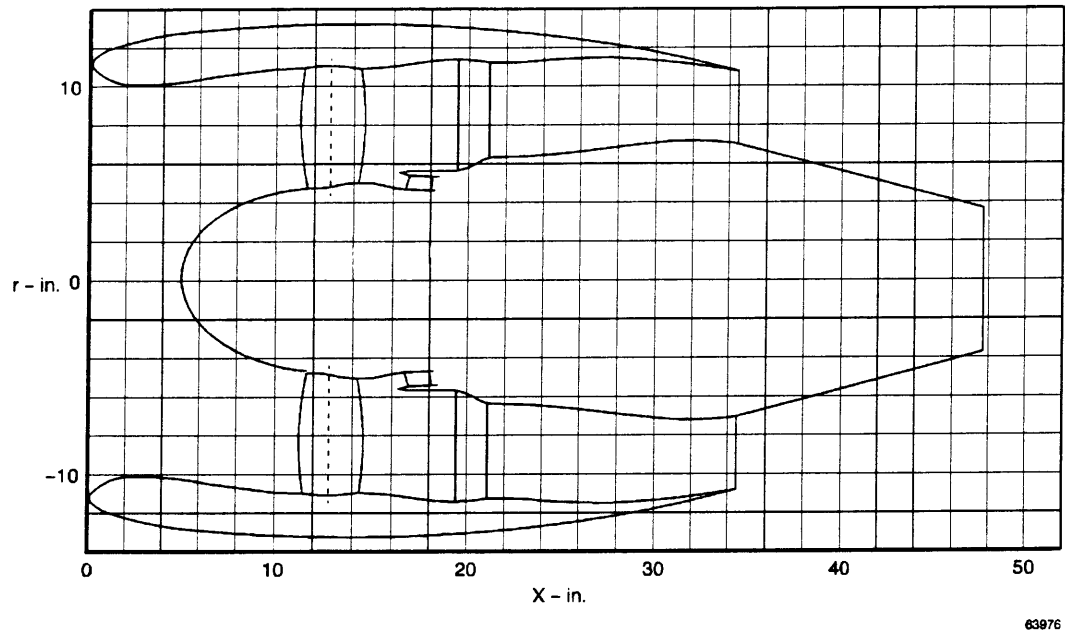
Figure 6-1. Low Noise Fan Nacelle

7. CONCLUSIONS

This report described the aerodynamic, acoustic, and structural design of the low noise fan model. Based on the design and analysis presented in each of these areas, the model is expected to meet all design requirements. Testing of this model will provide essential information on the validity of the design assumptions.

8. APPENDICES

Appendix A. Design Velocity Vector Listing

Table A-1. Definition of Parameters

Symbol	Definition
-1	Condition at the airfoil leading edge
-2	Condition at the airfoil trailing edge
SL	Streamline number
V	Velocity
VM	Meridional velocity
$V\theta$	Tangential velocity
U	Tangential velocity of rotor blade
EPSI	Cone angle of the flow (PHI)
B	Air angle measured from axial (BETA)
M	Mach number
TURN	Turning angle (B' minus B'-2*)
PCT TE SPAN	Percent span at trailing edge measured from hub to tip
N_{CORR} INLET	Corrected rotor angular velocity [viz, actual rpm divided by the square root of upstream total temperature over 288.2K (518.7R)]
W_{CORR} INLET	Corrected flow [actual mass flow multiplied by the square root of upstream total temperature over 288.2K (518.7R) and divided by the upstream total pressure over 10332 kg/m^2 (2116lb$_f$/ft^2)]

* Prime symbols indicate a quantity in the rotating frame, non-prime symbols indicate the stationary frame.

Table A-2. Fan Blade

DESIGN POINT   ROTOR

SL	V-1 M/SEC	V-2 M/SEC	VM-1 M/SEC	VM-2 M/SEC	VO-1 M/SEC	VO-2 M/SEC	U-1 M/SEC	U-2 M/SEC	V'-1 M/SEC	V'-2 M/SEC	VO'-1 M/SEC	VO'-2 M/SEC	EPSI-1 RADIAN	EPSI-2 RADIAN
1	217.8	204.2	217.8	186.7	0.0	82.8	111.8	118.0	244.8	190.0	-111.8	-35.2	0.1016	0.0573
2	216.0	208.9	216.0	186.3	0.0	94.6	118.8	124.7	246.5	188.7	-118.8	-30.0	0.1200	0.0533
3	215.3	214.0	215.3	185.9	0.0	106.0	125.9	131.4	249.4	187.6	-125.9	-25.4	0.1284	0.0526
4	215.0	226.7	215.0	185.0	0.0	131.0	147.0	151.5	260.5	186.1	-147.0	-20.5	0.1287	0.0566
5	213.2	230.2	213.2	184.7	0.0	137.4	175.2	178.2	276.0	189.2	-175.2	-40.8	0.1075	0.0566
6	211.2	228.3	211.2	185.5	0.0	133.2	189.3	191.6	283.6	194.5	-189.3	-58.4	0.0942	0.0502
7	208.7	227.1	208.7	187.3	0.0	128.4	203.4	205.0	291.4	202.4	-203.4	-76.6	0.0803	0.0391
8	205.6	226.3	205.6	190.3	0.0	122.4	217.5	218.4	299.3	213.1	-217.5	-95.9	0.0667	0.0237
9	204.1	224.8	204.1	191.4	0.0	117.9	224.5	225.1	303.4	219.3	-224.5	-107.2	0.0596	0.0132
10	202.8	220.2	202.8	188.9	0.0	113.2	231.6	231.7	307.8	223.0	-231.6	-118.5	0.0542	0.0011
11	202.6	211.5	202.6	180.0	0.0	111.1	238.6	238.4	313.0	220.5	-238.6	-127.3	0.0522	-0.0151

SL	B-1 degree	B-2 degree	B'-1 degree	B'-2 degree	M-1	M-2	M'-1	M'-2	TURN DEGREE
1	0.0	23.8	27.16	10.65	0.6677	0.6118	0.7505	0.5692	16.51
2	0.0	26.9	28.87	9.13	0.6618	0.6248	0.7554	0.5643	19.74
3	0.0	29.6	30.41	7.76	0.6596	0.6386	0.7641	0.5599	22.65
4	0.0	35.3	34.52	6.32	0.6585	0.6728	0.7978	0.5525	28.21
5	0.0	36.7	39.54	12.46	0.6527	0.6789	0.8447	0.5578	27.08
6	0.0	35.7	41.98	17.50	0.6460	0.6715	0.8674	0.5719	24.47
7	0.0	34.4	44.35	22.25	0.6376	0.6667	0.8903	0.5941	22.10
8	0.0	32.8	46.67	26.76	0.6274	0.6636	0.9133	0.6250	19.91
9	0.0	31.6	47.78	29.26	0.6223	0.6590	0.9253	0.6431	18.53
10	0.0	30.9	48.83	32.11	0.6183	0.6448	0.9384	0.6529	16.72
11	0.0	31.7	49.71	35.28	0.6175	0.6173	0.9541	0.6435	14.43

SL	V-1 ft/sec	V-2 ft/sec	VM-1 ft/sec	VM-2 ft/sec	VO-1 ft/sec	VO-2 ft/sec	U-1 ft/sec	U-2 ft/sec	V'-1 ft/sEC	V'-2 FT/SEC	VO'-1 FT/SEC	VO'-2 FT/SEC	EPSI-1 DEGREE	EPSI-2 DEGREE	PCT TE SPAN
1	714.5	670.0	714.5	612.5	0.0	271.5	366.8	387.1	803.1	623.3	-366.8	-115.6	5.824	3.285	0.0500
2	708.7	685.5	708.7	611.2	0.0	310.5	389.9	409.1	808.9	619.1	-389.9	-98.6	6.874	3.056	0.1000
3	706.5	702.0	706.5	609.8	0.0	347.7	413.0	431.1	818.4	615.5	-413.0	-83.3	7.354	3.012	0.1500
4	705.4	743.7	705.4	607.0	0.0	429.7	482.4	496.9	854.6	610.7	-482.4	-67.3	7.371	3.242	0.3000
5	699.7	755.4	699.7	606.1	0.0	450.8	574.8	584.7	905.5	620.7	-574.8	-133.9	6.160	3.240	0.5000
6	693.0	749.1	693.0	608.5	0.0	436.9	621.1	628.6	930.6	638.0	-621.1	-191.8	5.398	2.874	0.6000
7	684.7	745.1	684.7	614.6	0.0	421.2	667.3	672.5	956.1	664.0	-667.3	-251.3	4.603	2.241	0.7000
8	674.6	742.4	674.6	624.4	0.0	401.6	713.5	716.4	981.9	699.3	-713.5	-314.8	3.823	1.358	0.8000
9	669.5	737.4	669.5	627.9	0.0	386.7	736.7	738.4	995.4	719.7	-736.7	-351.7	3.418	0.754	0.8500
10	665.5	722.5	665.5	619.6	0.0	371.5	759.8	760.3	1010.0	731.5	-759.8	-388.8	3.106	0.063	0.9000
11	664.6	694.1	664.6	590.7	0.0	364.5	782.9	782.3	1027.0	723.5	-782.9	-417.8	2.989	-0.867	0.9500

NCORR INLET RPM	WCORR INLET LBM/SEC	WCORR INLET KG/SEC	PO/PO INLET
8396.50	91.8190	41.6488	1.2884

Table A-3. Fan Exit Guide Vane

DESIGN POINT   FEGV

SL	V-1 m/sec	V-2 m/sec	VM-1 m/sec	VM-2 m/sec	VO-1 m/sec	VO-2 m/sEC	EPSI-1 RADIAN	EPSI-2 RADIAN
1	158.3	141.7	121.6	141.7	101.4	0.0	0.1541	0.2046
2	171.6	148.7	134.1	148.7	107.0	0.0	0.1655	0.1916
3	183.7	156.2	144.9	156.2	112.8	0.0	0.1704	0.1778
4	211.2	177.2	166.7	177.2	129.6	0.0	0.1507	0.1337
5	221.4	185.7	179.3	185.7	129.9	0.0	0.1017	0.0772
6	221.1	188.1	181.5	188.1	126.2	0.0	0.0787	0.0521
7	218.7	190.0	181.5	190.0	121.9	0.0	0.0573	0.0281
8	212.8	189.0	178.6	189.0	115.8	0.0	0.0372	0.0051
9	206.0	185.0	173.1	185.0	111.8	0.0	0.0278	-0.0062
10	194.9	177.2	161.8	177.2	108.6	0.0	0.0182	-0.0183
11	178.8	165.2	142.7	165.2	107.7	0.0	0.0065	-0.0330

SL	B-1 DEGREE	B-2 DEGREE	M-1	M-2	TURN DEGREE
1	38.9	0.0	0.4642	0.4136	38.87
2	37.8	0.0	0.5038	0.4337	37.85
3	37.3	0.0	0.5398	0.4551	37.31
4	37.6	0.0	0.6213	0.5151	37.57
5	35.8	0.0	0.6501	0.5383	35.81
6	34.8	0.0	0.6480	0.5451	34.79
7	33.9	0.0	0.6398	0.5504	33.89
8	33.0	0.0	0.6212	0.5473	32.99
9	32.9	0.0	0.6001	0.5351	32.86
10	33.9	0.0	0.5655	0.5114	33.86
11	37.0	0.0	0.5160	0.4750	37.02

SL	V-1 FT/SEC	V-2 FT/SEC	VM-1 FT/SEC	VM-2 FT/SEC	VO-1 FT/SEC	VO-2 FT/SEC	PCT TE SPAN	EPSI-1 DEGREE	EPSI-2 DEGREE
1	519.5	464.9	398.9	464.9	332.7	0.0	0.0500	8.830	11.720
2	563.0	488.0	440.0	488.0	351.2	0.0	0.1000	9.480	10.975
3	602.6	512.4	475.6	512.4	370.1	0.0	0.1500	9.763	10.190
4	693.0	581.4	547.1	581.4	425.3	0.0	0.3000	8.637	7.658
5	726.5	609.1	588.4	609.1	426.2	0.0	0.5000	5.825	4.424
6	725.3	617.1	595.4	617.1	414.2	0.0	0.6000	4.510	2.984
7	717.5	623.4	595.6	623.4	400.1	0.0	0.7000	3.281	1.613
8	698.3	620.3	585.8	620.3	380.0	0.0	0.8000	2.133	0.293
9	676.0	606.9	567.9	606.9	366.7	0.0	0.8500	1.595	-0.357
10	639.3	581.3	530.9	581.3	356.2	0.0	0.9000	1.045	-1.049
11	586.6	542.1	468.2	542.1	353.4	0.0	0.9500	0.374	-1.892

NCORR INLET RPM	WCORR INLET LBM/SEC	WCORR INLET KG/SEC
8396.50	91.82	41.65

39

Table A-4. Core Stator

DESIGN POINT   CORE STATOR

SL	V-1 m/sec	V-2 m/sec	VM-1 m/sec	VM-2 m/sec	VO-1 m/sec	VO-2 m/sEC	EPSI-1 RADIAN	EPSI-2 RADIAN
1	160.4	130.3	139.9	130.3	78.4	0.0	-0.2593	-0.0425
2	162.8	134.1	141.9	134.1	79.7	0.0	-0.2522	-0.0437
3	165.1	137.8	143.9	137.8	80.9	0.0	-0.2451	-0.0449
4	172.6	148.8	150.2	148.8	84.9	0.0	-0.2293	-0.0482
5	183.0	163.1	159.1	163.1	90.3	0.0	-0.2202	-0.0514
6	188.2	169.8	163.6	169.8	93.0	0.0	-0.2194	-0.0527
7	193.8	176.4	168.4	176.4	95.8	0.0	-0.2198	-0.0537
8	199.5	182.7	173.4	182.7	98.7	0.0	-0.2216	-0.0545
9	203.0	185.9	176.6	185.9	100.1	0.0	-0.2384	-0.0549
10	207.6	189.1	181.1	189.1	101.6	0.0	-0.2814	-0.0550
11	212.2	192.3	185.6	192.3	103.0	0.0	-0.3244	-0.0552

SL	B-1 degree	B-2 degree	M-1	M-2	TURN DEGREE
1	29.8	0.0	0.4752	0.3834	29.78
2	29.8	0.0	0.4825	0.3945	29.79
3	29.8	0.0	0.4897	0.4056	29.79
4	29.8	0.0	0.5122	0.4389	29.82
5	29.9	0.0	0.5440	0.4823	29.91
6	30.0	0.0	0.5603	0.5026	29.95
7	30.0	0.0	0.5773	0.5225	29.99
8	30.0	0.0	0.5951	0.5419	30.00
9	30.0	0.0	0.6061	0.5516	30.00
10	30.0	0.0	0.6206	0.5614	30.03
11	30.1	0.0	0.6351	0.5712	30.11

SL	V-1 ft/sec	V-2 ft/sec	VM-1 ft/sec	VM-2 ft/sec	VO-1 ft/sec	VO-2 ft/sEC	PCT TE SPAN	EPSI-1 DEGREE	EPSI-2 DEGREE
1	526.1	427.7	459.0	427.7	257.2	0.0	0.0500	-14.856	-2.433
2	534.0	439.8	465.6	439.8	261.4	0.0	0.1000	-14.451	-2.503
3	541.8	452.0	472.3	452.0	265.6	0.0	0.1500	-14.045	-2.572
4	566.2	488.2	492.9	488.2	278.5	0.0	0.3000	-13.136	-2.760
5	600.3	535.3	522.0	535.3	296.3	0.0	0.5000	-12.619	-2.944
6	617.6	557.2	536.9	557.2	305.3	0.0	0.6000	-12.569	-3.017
7	635.8	578.6	552.6	578.6	314.4	0.0	0.7000	-12.595	-3.079
8	654.6	599.4	568.9	599.4	323.8	0.0	0.8000	-12.695	-3.124
9	666.2	609.9	579.6	609.9	328.4	0.0	0.8500	-13.659	-3.143
10	681.3	620.3	594.2	620.3	333.2	0.0	0.9000	-16.123	-3.152
11	696.3	630.8	608.8	630.8	337.9	0.0	0.9500	-18.587	-3.161

NCORR INLET rpm	WCORR INLET lbm/sec	WCORR INLET kg/sec
8396.50	91.82	41.65

Appendix B. Flowpath Coordinates

Table B-1. Fan Outer Flowpath

AXIAL	RADIUS		AXIAL	RADIUS		AXIAL	RADIUS
-12.75000	11.17150		-0.44360	11.06530		9.21092	11.28798
-12.74216	11.08857		-0.30420	11.07000		9.37866	11.29056
-12.71779	11.00376		-0.16490	11.07290		9.54846	11.29525
-12.67575	10.91779		-0.02550	11.07410		9.72058	11.30185
-12.61515	10.83151		0.11380	11.07360		9.89530	11.31015
-12.53545	10.74584		0.25310	11.07130		10.07286	11.31996
-12.43645	10.66178		0.39250	11.06720		10.25357	11.33105
-12.31841	10.58034		0.53180	11.06140		10.43769	11.34325
-12.18203	10.50253		0.67120	11.05380		10.62544	11.35633
-12.02843	10.42933		0.81050	11.04450		10.81713	11.37011
-11.85917	10.36163		0.94980	11.03340		11.01302	11.38437
-11.67617	10.30019		1.08920	11.02050		11.21337	11.39891
-11.48166	10.24563		1.22850	11.00580		11.41844	11.41354
-11.27806	10.19842		1.36790	10.98940		11.62853	11.42805
-11.06790	10.15882		1.50721	10.97110	FAN TE	11.84387	11.44223
-10.85373	10.12694		1.65878	10.97216		12.06474	11.45588
-10.63802	10.10270		1.83588	10.97521		12.29143	11.46881
-10.42310	10.08588		2.01306	10.98232		12.52417	11.48080
-10.21106	10.07613		2.19020	10.99080		12.76325	11.49166
-10.00375	10.07300		2.36724	10.99985		13.00893	11.50119
-9.72776	10.07508		2.54408	11.00980		13.26148	11.50917
-9.45176	10.08131		2.72078	11.02104		13.52117	11.51541
-9.17577	10.09164		2.89729	11.03393		13.78824	11.51970
-8.89977	10.10596		3.07360	11.04885		14.06299	11.52184
-8.62377	10.12416		3.24967	11.06616		14.34567	11.52164
-8.34778	10.14608		3.42549	11.08597		14.63657	11.51888
-8.07178	10.17151		3.60114	11.10800		14.93595	11.51337
-7.79579	10.20025		3.77658	11.13193		15.24404	11.50489
-7.51979	10.23202		3.95188	11.15744		15.56114	11.49326
-7.24380	10.26655		4.12702	11.18421		15.88751	11.47826
-6.96781	10.30354		4.30205	11.21193		16.22343	11.45969
-6.69182	10.34266		4.47701	11.24017		16.56917	11.43736
-6.41584	10.38357		4.65198	11.26818		16.92496	11.41105
-6.13985	10.42589		4.82704	11.29513		17.29109	11.38056
-5.86387	10.46926		5.00231	11.32018		17.66785	11.34570
-5.58788	10.51330		5.17787	11.34253		18.05547	11.30626
-5.31190	10.55762		5.35382	11.36133		18.45422	11.26204
-5.03591	10.60182		5.53021	11.37609		18.86441	11.21283
-4.75993	10.64551		5.70693	11.38736		19.28625	11.15843
-4.48394	10.68831		5.88387	11.39589		19.72005	11.09865
-4.20795	10.72984		6.06088	11.40241		20.16605	11.03326
-3.93196	10.76974		6.23792	11.40719		20.62453	10.96209
-3.65597	10.80765		6.41496	11.40986		21.09576	10.88491
-3.37998	10.84323		6.59200	11.41000	FEGV LE	21.58000	10.80153
-3.10398	10.87617		6.77390	11.40718			
-2.82799	10.90619		6.95575	11.40141			
-2.55199	10.93300		7.13751	11.39281			
-2.27600	10.95639		7.31915	11.38153			
-2.00000	10.97614		7.50061	11.36751			
-1.80643	10.98673		7.68184	11.35073			
-1.61266	10.99320		7.86302	11.33369			
-1.45879	10.99591		8.04434	11.31918			
-1.27962	11.00000	FAN LE	8.22600	11.31000	FEGV TE		
-1.14030	11.01530		8.38965	11.30471			
-1.00090	11.02880		8.55326	11.29925			
-0.86160	11.04060		8.71688	11.29415			
-0.72220	11.05060		8.88057	11.28994			
-0.58290	11.05880		9.04498	11.28770			

42

Table B-2. Fan Inner Flowpath

AXIAL	RADIUS
-7.74119	0.0
-7.74023	0.07657
-7.73735	0.15289
-7.73258	0.22894
-7.72591	0.30471
-7.71738	0.38019
-7.70698	0.45537
-7.69473	0.53025
-7.68066	0.60480
-7.66476	0.67902
-7.64706	0.75290
-7.62757	0.82642
-7.60630	0.89959
-7.58326	0.97238
-7.55847	1.04479
-7.53194	1.11681
-7.50369	1.18842
-7.47373	1.25962
-7.44207	1.33040
-7.40873	1.40073
-7.37372	1.47063
-7.33705	1.54006
-7.29874	1.60904
-7.25880	1.67753
-7.21724	1.74554
-7.17408	1.81304
-7.12933	1.88005
-7.08301	1.94653
-7.03513	2.01248
-6.98569	2.07789
-6.93473	2.14276
-6.88224	2.20706
-6.82824	2.27079
-6.77275	2.33395
-6.71578	2.39651
-6.65735	2.45846
-6.59746	2.51981
-6.53613	2.58053
-6.47338	2.64062
-6.40921	2.70007
-6.34364	2.75886
-6.27669	2.81698
-6.20837	2.87443
-6.13869	2.93120
-6.06767	2.98727
-5.99531	3.04263
-5.92164	3.09728
-5.84666	3.15120
-5.77039	3.20438
-5.69285	3.25682
-5.61404	3.30849
-5.53398	3.35940
-5.45269	3.40952
-5.37017	3.45886
-5.28645	3.50740
-5.20153	3.55512
-5.11542	3.60203
-5.02815	3.64810

AXIAL	RADIUS	
-4.93973	3.69333	
-4.85016	3.73771	
-4.75947	3.78123	
-4.66766	3.82387	
-4.57475	3.86563	
-4.48076	3.90649	
-4.38569	3.94645	
-4.28956	3.98550	
-4.19239	4.02361	
-4.09418	4.06080	
-3.99496	4.09703	
-3.89473	4.13232	
-3.79350	4.16663	
-3.69130	4.19996	
-3.58813	4.23231	
-3.48402	4.26366	
-3.37896	4.29400	
-3.27298	4.32332	
-3.16609	4.35161	
-3.05831	4.37886	
-2.94964	4.40506	
-2.84010	4.43020	
-2.72970	4.45427	
-2.61846	4.47725	
-2.50639	4.49914	
-2.39351	4.51993	
-2.27982	4.53961	
-2.16535	4.55816	
-2.05010	4.57558	
-1.93409	4.59186	
-1.81733	4.60697	
-1.69988	4.62100	
-1.58227	4.63476	
-1.46466	4.64853	
-1.34705	4.66230	
-1.22944	4.67607	
-1.08416	4.69000	FAN LE
-0.99463	4.69671	
-0.87629	4.70176	
-0.75779	4.70533	
-0.63910	4.70777	
-0.52019	4.70943	
-0.40116	4.71115	
-0.28229	4.71462	
-0.16388	4.72159	
-0.04626	4.73382	
0.07029	4.75292	
0.18586	4.77832	
0.30081	4.80779	
0.41551	4.83904	
0.53034	4.86978	
0.64565	4.89775	
0.76177	4.92095	
0.87871	4.93930	
0.99634	4.95348	
1.11450	4.96420	
1.23311	4.97215	
1.35640	4.97803	FAN TE

AXIAL	RADIUS	
1.47104	4.98254	
1.59011	4.98632	
1.70911	4.98924	
1.82797	4.99064	
1.94661	4.98985	
2.06496	4.98620	
2.18295	4.97901	
2.30049	4.96766	
2.41760	4.95216	
2.80000	4.86000	
3.24000	4.73000	
3.50000	4.64000	
3.89000	4.51500	S1 LE
4.24200	4.43000	
4.67300	4.38700	S1 TE
5.17000	4.40000	
5.91000	4.47500	
6.74000	4.57500	
7.80000	4.70000	
10.1000	4.70000	
12.2100	4.70000	
27.6300	4.70000	
34.0000	4.70000	

Table B-3. Fan Duct Inner Flowpath

AXIAL	RADIUS		AXIAL	RADIUS		AXIAL	RADIUS
3.74000	5.55000		15.52074	6.95323		31.15733	4.66212
3.75000	5.58100		15.79044	6.98597		31.42587	4.59516
3.76000	5.59450		16.06020	7.01760		31.69441	4.52821
3.78000	5.61600		16.33003	7.04788		31.96295	4.46125
3.83000	5.65400		16.59995	7.07658		32.23149	4.39430
3.90000	5.68850		16.86996	7.10349		32.50003	4.32734
4.00000	5.72600		17.14008	7.12836		32.76859	4.26039
4.10000	5.75300		17.41032	7.15097		33.03712	4.19343
4.20000	5.77450		17.68071	7.17109		33.30566	4.12648
4.30000	5.79100		17.95123	7.18849		33.57420	4.05952
5.25000	5.81000		18.22192	7.20294		33.84274	3.99257
5.60000	5.81000		18.49278	7.21421		34.11128	3.92561
5.99000	5.81000		18.76382	7.22207		34.37982	3.85866
6.30000	5.81000		19.03506	7.22629		34.64836	3.79170
6.59200	5.81000	FEGV LE	19.30650	7.22664		34.91690	3.72475
6.77400	5.82900		19.57817	7.22289			
6.97400	5.87900		19.85008	7.21481			
7.17400	5.95200		20.12224	7.20218			
7.37400	6.03900		20.39465	7.18476			
7.57400	6.12700		20.66734	7.16232			
7.77400	6.21000		20.94031	7.13463			
7.97400	6.28200		21.21358	7.10147			
8.22600	6.35000	FEGV TE	21.48712	7.06231			
8.37400	6.37600		21.75836	7.00554			
8.57400	6.39900		22.02692	6.93859			
8.77400	6.41400		22.29546	6.87163			
8.97400	6.42600		22.56400	6.80468			
9.17400	6.43900		22.83253	6.73772			
9.37400	6.45100		23.10107	6.67077			
9.57400	6.46400		23.36961	6.60381			
9.77400	6.47500		23.63815	6.53686			
9.97400	6.48600		23.90671	6.46990			
10.17400	6.49500		24.17525	6.40295			
10.37400	6.50400		24.44379	6.33599			
10.57400	6.51200		24.71233	6.26904			
10.77400	6.52000		24.98087	6.20208			
11.97400	6.52800		25.24940	6.13513			
11.17400	6.53700		25.51796	6.06817			
11.37400	6.54500		25.78650	6.00122			
11.57400	6.55500		26.05504	5.93426			
11.77400	6.56600		26.32358	5.86731			
11.97400	6.57800		26.59212	5.80035			
12.17400	6.59100		26.86066	5.73340			
12.37400	6.60600		27.12921	5.66644			
12.57400	6.62300		27.39775	5.59949			
12.77400	6.64000		27.66629	5.53253			
12.97400	6.65900		27.93483	5.46558			
13.17400	6.67900		28.20337	5.39862			
13.37400	6.69900		28.47191	5.33167			
13.57400	6.72100		28.74046	5.26471			
13.77400	6.74300		29.00900	5.19776			
13.97400	6.76600		29.27754	5.13080			
14.17400	6.79000		29.54608	5.06385			
14.37400	6.81400		29.81462	4.99689			
14.57400	6.83800		30.08316	4.92994			
14.71187	6.85064		30.35170	4.86298			
14.98146	6.88534		30.62025	4.79603			
15.25109	6.91961		30.88879	4.72907			

Table B-4. Core Outer Flowpath

AXIAL	RADIUS		
3.74000	5.55000		
3.75000	5.49900		
3.76000	5.48300		
3.78000	5.46000		
3.83000	5.42200		
3.90000	5.38450		
4.00000	5.34550		
4.12000	5.31000	S1	LE
4.51300	5.24200		
4.90300	5.20200	S1	TE
5.41000	5.20500		
5.91000	5.27500		
6.74000	5.36400		
7.80000	5.41000		
10.1000	5.41000		
12.2100	5.41000		
27.6300	5.41000		
34.0000	5.96750		

Appendix C. Disk Design Stresses

Properties of Parts Contributions to Disk Dead Load

Component	ρ (lb/in³)	V (in³)	CG Radius (in)	Count	Hoop Direction Area (in²)
Tie Bolt Head	0.297	0.072	3.695	18	N/A
Tie Bolt Nut	0.297	0.194	3.695	18	N/A
Disk Rear Half Snap Bolt	0.283	0.076	2.670	18	N/A
Blade Pin	0.285	0.041	4.340	18	N/A
Spar & Shell	*	1.863	7.384	18	N/A
Platform & Tangs	0.160	0.305	4.614	18	N/A
Receiver	0.160	0.633	3.477	18	N/A
Receiver Hole	0.283	0.463	3.742	18	0.764
Disk Front Half (w/o receiver hole)	0.283	N/A	3.666	1	1.446
Disk Rear Half (w/o receiver hole)	0.283	N/A	4.023	1	1.860
Tie Rod Hole Front Half (w/o receiver hole)	*	N/A	3.695	18	0.540
Tie Rod Hole Rear Half (w/o receiver hole)	*	N/A	3.695	18	0.373

*area or volume weighted density to be calculated due to different materials

N/A = not applicable
g_c = 386.4 in/sec²
tie bolt diameter = 0.4375 in
spar volume = 0.218 in³
spar density = 0.160 lb/in³
shell volume = 1.645 in³
shell density = 0.058 lb/in³

Calculate Weighted Average Densities of Spar/Shell and Tie Rod/Tie Rod Disk Ring

Spar/Shell Volume Weighted Density

$$\rho = \frac{\sum \rho_i V_i}{\sum V_i} = \frac{0.160(0.218) + 0.058(1.645)}{0.218 + 1.645} = 0.070 \text{ lb / in}^2$$

Tie Rod/ Tie Rod Disk Ring Area Weighted Density

$$r_o = \text{disk ring outer radius} = R_{cg.bolt} + \frac{D_{bolt}}{2} = 3.695 + \frac{0.4375}{2} = 3.914 \text{ in}$$

$$r_i = \text{disk ring inner radius} = R_{cg.bolt} + \frac{D_{bolt}}{2} = 3.695 + \frac{0.4375}{2} = 3.476 \text{ in}$$

$$A_{ring} = \text{disk ring area} = \pi(r_o^2 - r_i^2) = \pi(3.914^2 - 3.476^2)^2 = 10.157 \text{ in}^2$$

$$A_{bolts} = \text{total bolt cross section area} = N\pi \frac{D_{bolt}^2}{4} = 18\pi \frac{0.4375^2}{4} = 2.706 \text{ in}^2$$

$$\rho = \frac{\sum \rho_i A_i}{\sum A_i} = \frac{0.283(10.157 - 2706) + 0.297(2.706)}{10.157} = 0.287 \text{ lb / in}^3$$

Calculate Component Redline Centrifugal Pulls

$$pull = mr_{cg}\omega^2 = N\frac{\rho V}{g_c}r_{cg}\left(\frac{rpm}{60}(2\pi)\right)^2$$

Tie Bolt Heads

$$pull = 18\frac{(0.297)(0.072)}{397/4}(3.695)\left(\frac{10836}{60}(2\pi)\right)^2 = 4740 \text{ lb}_f$$

Tie Bolt Nuts

$$pull = 18\frac{(0.297)(0.194)}{386.4}(3.695)\left(\frac{10937}{60}(2\pi)\right)^2 = 12770 \text{ lb}_f$$

47

Disk Rear Half Snap Bolts

$$pull = 18\frac{(0.283)(0.076)}{386.4}(2.670)\left(\frac{10836}{60}(2\pi)\right)^2 = 3445 \text{ lb}_f$$

Blade Pins

$$pull = 18\frac{(0.285)(0.041)}{386.4}(4.340)\left(\frac{10836}{60}(2\pi)\right)^2 = 3042 \text{ lb}_f$$

Spars & Shells

$$pull = 18\frac{(0.070)(1.645+0.218)}{386.4}(7.384)\left(\frac{10836}{60}(2\pi)\right)^2 = 57761 \text{ lb}_f$$

Platforms & Tangs

$$pull = 18\frac{(0.160)(0.305)}{386.4}(4.614)\left(\frac{10836}{60}(2\pi)\right)^2 = 135061 \text{ lb}_f$$

Receivers

$$pull = 18\frac{(0.160)(0.633)}{386.4}(3.477)\left(\frac{10836}{60}(2\pi)\right)^2 = 21123 \text{ lb}_f$$

Disk Ring Without Receiver Holes

$$V = V_{ring} - V_{receiver\,holes} = 2\pi r_{cg}A - NV_{receiver\,hole}$$

$$= 2\pi(3.742)(0.764) - 18(0.463) = 9631 \text{ in}^3$$

$$pull = (0.283)\frac{(9.631)(3.742)}{386.4}\left(\frac{10836}{60}(2\pi)\right)^2 = 33987 \text{ lb}_f$$

48

Disk Ring and Tie Rods

$$V = 2\pi r_{cg} A = 2\pi(3.695)(0.540 + 0.373) = 21.197 \text{ in}^3$$

$$pull = \frac{(0.287)(21.197)}{386.4}(3.695)\left(\frac{10836}{60}(2\pi)\right)^2 = 74907 \text{ lb}_f$$

Live Disk

$$A_{\text{live disk}} = A_{\text{front half}} + A_{\text{rear half}} - A_{\text{tie bolt}} = 1.446 + 1.860 - 0.540 - 0.373$$

$$= 2.393 \text{ in}^2$$

$$r_{cg} = \frac{\sum A_i r_i}{\sum A_i} = \frac{1.446(3.666) + 1.860(4.023) - (0.540 + 0.373)(3.695)}{2.393}$$

$$= 3.932 \text{ in}$$

$$V = 2\pi r_{cg} A = 2\pi(3.932)(2.393) = 59.127 \text{ in}^3$$

$$pull = \frac{(0.283)(59.127)}{397.4}(3.932)\left(\frac{10836}{60}(2\pi)\right)^2 = 219250 \text{ lb}_f$$

Average Tangential Stress

$$\sigma_{t,\text{average}} = \frac{pull_{\text{dead load}} + pull_{\text{live disk}}}{2\pi A_{\text{live disk}}}$$

$$= \frac{225281 + 219250}{2\pi(2.393)} = 29565 \text{ psi}$$

Allowable Tangential Stress

$$\sigma_{t,allowable} = \frac{M.U.F.(\sigma_{ult})}{\text{Safety Factor}}$$

$$= \frac{0.7(150000)}{1.5}$$

$$= 70000 \text{ psi}$$

REPORT DOCUMENTATION PAGE

Public reporting burden for this collection of information is estimated to average 1 hour per response, including the time for reviewing instructions, searching existing data sources, gathering and maintaining the data needed, and completing and reviewing the collection of information. Send comments regarding this burden estimate or any other aspect of this collection of information, including suggestions for reducing this burden, to Washington Headquarters Services, Directorate for Information Operations and Reports, 1215 Jefferson Davis Highway, Suite 1204, Arlington, VA 22202-4302, and to the Office of Management and Budget, Paperwork Reduction Project (0704-0188), Washington, DC 20503.

1. AGENCY USE ONLY (Leave blank)	2. REPORT DATE March 1995	3. REPORT TYPE AND DATES COVERED Final Contractor Report

4. TITLE AND SUBTITLE

Low Noise Research Fan Stage Design

5. FUNDING NUMBERS

WU–538–03–11
NAS3–26618

6. AUTHOR(S)

David E. Hobbs, Robert J. Neubert, Eric W. Malmborg,
Daniel H. Philbrick, and David A. Spear

7. PERFORMING ORGANIZATION NAME(S) AND ADDRESS(ES)

United Technologies Corporation
Pratt & Whitney
East Hartford, Connecticut 06108

8. PERFORMING ORGANIZATION REPORT NUMBER

E–9125

9. SPONSORING/MONITORING AGENCY NAME(S) AND ADDRESS(ES)

National Aeronautics and Space Administration
Lewis Research Center
Cleveland, Ohio 44135–3191

10. SPONSORING/MONITORING AGENCY REPORT NUMBER

NASA CR–195382

11. SUPPLEMENTARY NOTES

Project Manager, Robert J. Jeracki, Propulsion Systems Division, organization code 5940, (216) 433–3917.

12a. DISTRIBUTION/AVAILABILITY STATEMENT

Unclassified - Unlimited
Subject Category: 07   Distribution: Nonstandard

This publication is available from the NASA Center for AeroSpace Information, (301) 621–0390.

12b. DISTRIBUTION CODE

13. ABSTRACT (Maximum 200 words)

This report describes the design of a Low Noise ADP Research Fan stage. The fan is a variable pitch design which is designed at the cruise pitch condition. Relative to the cruise setting, the blade is closed at takeoff and opened for reverse thrust operation. The fan stage is a split flow design with fan exit guide vanes and core stators. This fan stage design was combined with a nacelle and engine core duct to form a powered fan/nacelle, subscale model. This model is intended for use in aerodynamic performance, acoustic and structural testing in a wind tunnel. The model has a 22–inch outer fan diameter and a hub-to-top ratio of 0.426 which permits the use of existing NASA fan and cowl force balance designs and rig drive system. The design parameters were selected to permit valid acoustic and aerodynamic comparisons with the PW 17–inch rig previously tested under NASA contract. The fan stage design is described in detail. The results of the design axisymmetric analysis at aerodynamic design condition are included. The structural analysis of the fan rotor and attachment is described including the material selections and stress analysis. The blade and attachment are predicted to have adequate low cycle fatigue life, and an acceptable operating range without resonant stress or flutter. The stage was acoustically designed with airfoil counts in the fan exit guide vane and core stator to minimize noise. A fan-FEGV tone analysis developed separately under NASA contract was used to determine these airfoil counts. The fan stage design was matched to a nacelle design to form a fan/nacelle model for wind tunnel testing. The nacelle design was developed under a separate NASA contract. The nacelle was designed with an axisymmetric inlet, cowl and nozzle for convenience in testing and fabrication. Aerodynamic analysis of the nacelle confirmed the required performance at various aircraft operating conditions.

14. SUBJECT TERMS

Turbofan; Low noise; Variable pitch; Low pressure ratio

15. NUMBER OF PAGES

60

16. PRICE CODE

A04

17. SECURITY CLASSIFICATION OF REPORT	18. SECURITY CLASSIFICATION OF THIS PAGE	19. SECURITY CLASSIFICATION OF ABSTRACT	20. LIMITATION OF ABSTRACT
Unclassified	Unclassified	Unclassified	